Link Between Opaque Cloud Properties and Atmospheric Dynamics in Observations and Simulations of Current Climate in the Tropics, and Impact on Future Predictions

Miguel Perpina, Vincent Noël, Helene Chepfer, Rodrigo Guzman, Artem Feofilov

Link between opaque cloud properties and atmospheric dynamics in observations and simulations of current climate in the Tropics, and impact on future predictions

Perpina Miguel[(1)], Noel Vincent[(2)], Chepfer Helene[(3)], Guzman Rodrigo[(3)] and Feofilov G. Artem[(3)]

[(1)] CNES/Laboratoire d'Aérologie, Paul Sabatier University, Toulouse, France (Miguel PERPINA: miguel.perpina@aero.obs-mip.fr)

[(2)] CNRS/Laboratoire d'Aérologie, Toulouse, France (Vincent NOEL: vincent.noel@aero.obs-mip.fr)

[(3)] LMD/IPSL, École Polytechnique, Institut Polytechnique de Paris, ENS, PSL Université, Sorbonne Université, CNRS, Palaiseau France (Helene Chepfer: chepfer@lmd.polytechnique.fr; Rodrigo GUZMAN: rodrigo.guzman@lmd.polytechnique.fr; Artem G. Feofilov: artem.feofilov@lmd.polytechnique.fr)

Key points:

- We document how both models predict cloud properties in the present and in a future, warmer climate with weakened Walker/Hadley circulation
- Both models show cloud properties evolve differently with vertical wind speeds smaller or larger than 20hPa/day
- Cloud properties that suffer from biases in model simulations of current climate are affected by large changes in the future climate

Abstract

Using spaceborne lidar observations and reanalyses (2008-2014), we relate the vertical wind speed at 500 hPa (ω_{500}), indicator of atmospheric circulation, to properties of opaque clouds (altitude and cover) and to the Cloud Radiative Effect (CRE) in the Tropics. We confront those observations with simulations by IPSL-CM6 and CESM1 climate models using early 21st century emissions. Both models overestimate the average opaque cloud cover. IPSL-CM6 puts high opaque clouds too high (+2km), especially in ascendance. CESM1 overestimates the intermediate opaque cloud cover and underestimates small and large opaque cloud covers. Both models agree that cloud properties behave differently at wind speed above (strong subsidence) or below (weak subsidence and ascendance) 20hPa/day. In future climate (2089-2095), variables affected by biases in current climate are affected by notable changes: IPSL-CM6 puts high opaque clouds even higher (+2km) while opaque cloud cover above 30% decreases and below 30% increases in CESM1. Both models predict very little change in the average net CRE in the future. We find that predicted changes of cloud properties can be regionally driven by dynamic or thermodynamic changes, depending on the relationship between opaque cloud altitude and ω_{500} in the model. Overall, most changes are due to thermodynamic changes in the relationship between cloud property and atmospheric dynamics.

Plain Language Summary

The largest incertitude on climate predictions comes from our poor understanding of how clouds will react to a warmer climate. A long-term record of cloud detections by active sensors, such as lidars, will enable measuring the clouds vertical distribution, one of the properties most sensitive to global warming. Here we investigate how two climate models predict the evolution of the vertical distribution of clouds, in relation to the predicted evolution of large-scale air motions in the Tropics. We discuss the changes predicted by the models in future climate conditions for cloud properties, and how well they simulate them in current climate conditions, compared to current retrievals from satellite sensors. We also find that when models generate upward or downward air motions, they move opaque clouds higher or lower in very different ways. This explains why, even if both models similarly predict that tropical atmospheric circulation will slow down in the future, they predict different changes in cloud altitude.

1 Introduction

Climate models predict a weakening of the tropical atmospheric circulation (Kjellsson 2015), more specifically a slowdown of Hadley and Walker circulations (Vecchi and Soden, 2006; Lu et al., 2007; Birner, 2010; Davis and Rosenlof, 2012). The Hadley cells are maintained by convection, and many studies predict that in a warming climate, convection will weaken due to changes in 1) the atmospheric hydrological cycle (Held and Soden, 2006), 2) the mean advection of stratification, which implies a cold/warm advection in the tropical troposphere in convective/subsidence regions (Ma et al., 2012), or 3) the radiative cooling in the upper atmosphere (Bony et al., 2013). Chou et al. (2009) showed that convection will weaken along the edges of convection regions due to advection of dry air from subsidence regions towards convective regions: the “upped-ante” mechanism. Ma et al. (2012) suggested that a warming of subsidence regions could strengthen the frequency of the ascendance in regions today dominated by subsidence. Cloud formation and distribution in the tropics, which are largely driven by vertical movements, will be impacted by these predicted changes (e.g. Cess et al., 1989; Stephens, 2005; Zelinka and Hartmann, 2011; Su et al., 2014).

Many climate models predict that global warming will have a major impact on cloud properties (e.g. Wetherald and Manabe, 1988; Ramanathan et al., 1989; Mitchell et al., 1989; Colman, 2003; Ringer et al., 2006; Webb et al., 2006; Vial et al., 2013; Vaillant de Guélis et al., 2018; Zelinka et al., 2020), including their geographic and vertical distribution. Climate feedbacks from clouds, which amplify warming when positive (Hansen et al., 1984), are today the main source of uncertainty in climate forecasts (e.g Vial et al., 2013; Webb et al., 2013; Caldwell et al., 2016; Ceppi et al., 2017, Zelinka et al. 2020). Tropical clouds play a key role in the redistribution of solar energy (Cesana et al., 2012; Dufresne and Bony, 2005; Lu et al, 2007; Kjellsson, 2014), and their evolution will likely affect climate. Therefore, it is crucial to better understand how tropical clouds will evolve in a changing climate.

Among cloud properties, the vertical distribution is sensitive to climate change (Hartmann and Larson, 2012; O'Gorman and Singh, 2013; Chepfer et al., 2014; Vaillant de Guélis et al., 2018). Active sensors integrated into satellites, such as CALIOP (Cloud-Aerosol LIdar with Orthogonal Polarization; Winker et al., 2009), make it possible to obtain a detailed vertical distribution of clouds. CALIOP measurements and calibration are more stable over time and more precise than passive remote sensing satellite detectors (Winker et al., 2017; Chepfer et al., 2018). CALIOP observations can be simulated in the atmospheric conditions predicted by climate models using lidar simulators (Chepfer et al., 2008). Chepfer et al. (2018) showed that, assuming model predictions are correct, observations from space lidars could monitor changes in the vertical distribution of tropical clouds in a way that could provide information on how clouds will impact the future climate.

One of the main influences clouds have on the climate system is their Cloud Radiative Effect, or CRE. A positive Top Of the Atmosphere (TOA) CRE means that clouds warm the climate system. Conversely, a negative TOA CRE means clouds cool the climate system. Zelinka et al. (2012a) quantified how cloud cover, altitude, and optical depth contribute to the cloud radiative response. Zelinka et al. (2016) isolated the role of cloud cover and cloud altitude, separating high and low clouds. In the infrared, or longwave (LW), clouds always have a warming effect ($CRE_{LW}>0$) because they absorb a part of the upwelling radiation emitted by the Earth and reemit a part of it downwards, thus letting less energy escape to space. Opaque clouds provide the largest contribution to TOA CRE_{LW}: when opaque cloud cover is large, CRE_{LW} is large (Vaillant de Guélis et al., 2017a). At global scale, Vaillant de Guélis et al. (2017b) showed that opaque clouds contribute to 82% and thin clouds to 18% of the mean observed LW CRE. Higher opaque clouds also lead to a stronger CRE_{LW}. In the visible, or shortwave (SW), clouds almost always have a cooling effect ($CRE_{SW}<0$) because they reflect a part of the solar radiation back to space. The SW CRE is directly proportional to the cloud optical depth (Yokohata et al., 2005; Taylor et al., 2007, Dupont et al. 2008), thus optically thin clouds contribute less to the SW CRE than opaque clouds, supposing equivalent cloud covers as in observations (Guzman et al., 2017). As the cover of opaque clouds increases, so will their albedo

effect, and the CRE_{SW} will get increasingly negative. Thus opaque clouds are the main contributors to the CRE in the Tropics.

Understanding how models predict cloud vertical distribution will evolve in the future has implications for how models predict the TOA CRE will evolve in the future (e.g. Bony et al., 2006; Soden and Held 2006; Soden et al., 2008; Boucher et al., 2013). Many studies show that cloud altitude change is the dominant contributor to the LW cloud feedback (e.g. Schneider, 1972; Cess, 1975; Hansen et al., 1984; Wetherald and Manabe, 1988; Cess et al., 1996; Hartmann and Larson, 2002; Zelinka et al., 2016). Vaillant de Guélis et al. (2018) showed that changes in altitude and cover of opaque clouds are the main drivers of CRE change in the Tropics on short timescales. At this point, however, it is still unclear how observing short-term, intra-decadal changes in cloud properties might reveal the evolution of the CRE in future climate conditions, given the long-term, multi-decadal changes in dynamical conditions of the tropics.

This paper has three goals. First, based on satellite observations and reanalyses (section 2), we establish the relationship between atmospheric dynamic circulation, opaque cloud properties and TOA CRE (section 3). Second, we compare this observed relationship with the one found in climate model simulations of current climate conditions (section 4). Third, we investigate how model biases in present climate conditions relate to their predictions in a warmer climate (section 5). All analyses are ocean only, to help interpretation of our results in regard of recent studies using lidar-derived opaque cloud properties (Vaillant de Guélis et al., 2017a, b, 2018; Höjgård-Olsen et al., 2020).

2 Data

In this study, we use cloud observations (section 2.1) from space lidar, vertical wind speed from reanalysis, flux observations from space radiometer. On the modeling side (section 2.2), we use climate simulations together with a lidar simulator in the present climate as well as in a warmer climate.

2.1 Observations

2.1.1 Cloud observations: CALIPSO-GOCCP Spaceborne Lidar Data

We use 7 years of CALIPSO observations (2008-2014) from the GOCCP product (GCM-Oriented CALIPSO Cloud Product, Chepfer et al., 2010, 2013). CALIPSO has been collecting data since 2006, but in November 2007 the satellite tilt was changed from 0.3° to 3° off-nadir. This change in CALIPSO's pointing direction can create discontinuities in retrieved cloud properties, in the Tropics and elsewhere (Hu et al., 2007), so we only consider observations starting in 2008. GOCCP variables are derived from CALIPSO level 1, vertical profiles measured every 330m at 30m-180m vertical resolution. We used GOCCP V.3.1.2 (Chepfer et al., 2010) variables consistent with the COSP1.4 lidar simulator outputs (section 2.2.2). From GOCCP data, we used 2 variables aggregated and averaged over monthly periods on 2°x2° lat-lon grid cells and on a 480m regular vertical resolution grid, that describe the properties of opaque clouds.

Opaque clouds are defined as clouds which totally attenuate the incoming lidar laser beam and do not let any of it pass through as direct transmission. Their optical depth is typically larger than 3 in the visible and an infrared (IR) emissivity close to 1; they are identified when the surface echo cannot be found in full-resolution signal profiles from the space lidar (Guzman et al., 2017). In this study, we use two lidar-derived properties of opaque clouds:

- The opaque cloud cover, named Copaque.

- The opaque cloud altitude, named Zopaque, which describes the altitude below which the lidar is fully attenuated and is directly linked to the LW TOA radiative flux (Chepfer et al., 2014; Vaillant de Guélis et al., 2017a; Guzman et al., 2017). The GOCCP Zopaque calculation algorithm is based on detecting the altitude where the lidar signal is totally attenuated. This attenuation is integrated over the entire column from the top, and can be due to a single cloud layer or multiple cloud layers. In a given profile, the Zopaque can be very low (e.g. 2 km) while thin high clouds can be present. When a situation combines low level opaque clouds with optically thin high clouds, the lidar will penetrate the high clouds and will get fully attenuated in the lower cloud. Compared to the situation with low opaque clouds only, this would marginally rise the altitude of opacity. De Guélis et al. (2017a) found that taking into account the optical depth of thinner clouds overlapping an opaque cloud when calculating the cloud radiative effect only provides marginal improvement.

Zopaque and Copaque have been used in several recent studies to understand interactions between clouds and radiation (e.g. Vaillant de Guélis et al., 2017a and b, 2018; Morrisson et al., 2018, 2019; Frey et al., 2018; Lacour et al., 2017, 2018; Chepfer et al., 2014, 2017, 2019).

2.1.2 Vertical wind speed: ERA5 reanalysis

To evaluate convection intensity, we use the vertical velocity at 500 hPa, ω_{500}. Averaged over a month, it is a good indicator of the ascending/subsiding air motion (Bony et al., 2004). Ascending air motion is identified by negative wind speeds at 500 hPa ($\omega_{500}<0$) and subsidence air motions by positive wind speeds at 500 hPa ($\omega_{500}>0$). Here, we use 7 years (2008-2014) of ω_{500} from fifth-generation reanalysis from ECMWF (European Centre for Medium-Range Weather Forecasts) ERA-5 (Hersbach et al., 2020).

These data are produced from the combination of a model of weather forecasts and observations. These ERA5 reanalyses are provided hourly on a 0.28°x0.28° longitude-latitude mesh and 137 vertical levels of varying pressure. We extracted the vertical velocity at 500 hPa and averaged it on the GOCCP horizontal resolution: 2°x2° every month.

2.1.3 Radiative flux: CERES Spaceborne Radiometer

In the present study, we used 7 years (2008-2014) of TOA CRE from the Clouds and the Earth's Radiant Energy System (CERES) Energy Balanced and Filled (EBAF) top-of-atmosphere (TOA) data product version 4.1 (Loeb et al., 2018; Kato et al., 2018). It is produced using 2 CERES instruments from two satellite platforms (Aqua and Terra), that measure SW, LW and total fluxes at TOA. These measurements are monthly averaged on a 1°x1° longitude-latitude grid.

2.2 Simulations

2.2.1 General Circulation Models: CESM1 and IPSL-CM6

In the present study we considered climate predictions from two general circulation models.

The first is the Community Earth System Model version 1 (CESM1), integrating the Community Atmosphere Model version 5 (CAM5), developed by NCAR (National Center of Atmospheric Research). CESM1-CAM5 participated in the fifth phase of the Coupled Model Intercomparison Project (CMIP5, Taylor et al. 2012). We used CESM1 data on a grid with a spatial resolution of 1.25° x 0.94°, and 40 vertical levels. The second model is IPSL-CM6, the latest version of the IPSL (Institut Pierre-Simon Laplace) climate model participated in the sixth phase of CMIP (Eyring et al., 2016).. We used IPSL-CM6 data on a grid with a spatial resolution of 1.27 ° x2.5 °, and 79 pressure levels.

According to Table 1, both models have a rather large equilibrium climate sensitivity (ECS) but ECS and cloud feedback values all fall in the range of CMIP6 multimodel means for both models. IPSL-CM6 appears as the most sensitive, with the strongest LW cloud feedbacks.

	Equilibrium Climate Sensitivity (K)	Cloud Feedback Total (W/m²/K)	Cloud Feedback SW (W/m²/K)	Cloud Feedback LW (W/m²/K)
CESM1-CAM5	4.1	+0.52	+0.42	+0.10
IPSL-CM6	4.6	+0.38	+0.13	+0.25
Multimodel mean interval CMIP6	2.6 to 4.8	+0.06 to +0.78	-0.39 to +0.59	+0.06 to 0.58

Table 1: Climate sensibility (K) and Cloud feedback Total, SW and LW (W/m²/K) for CESM1 and IPSL-CM6. Adapted from Gettelman et al., 2019, Meehl et al. 2020, and Zelinka et al., 2020.

For both models we considered 88 years of predictions, starting in 2008 as the observations and ending in 2095. Since CESM1 is a CMIP5 model and the historical period ends in 2005 for CMIP5 (Taylor et al., 2011), historical runs do not exist for later years in CESM1. However, the cumulative CO2 emissions observed during the 2008-2014 period are closest to the RCP8.5 scenario (Schalwm et al., 2020), and we used that scenario for CESM1 simulations over the 2008-2014 period. For the CMIP6 model IPSL-CM6, we used available historical runs for IPSL-CM6 over the period 2008-2014. For future climate conditions, both models were forced under the Representative Concentration Pathway (RCP) 8.5 scenario, the highest emissions and radiative forcing scenario of the Intergovernmental Panel on Climate Change exercise (Riahi et al., 2011). In the rest of the paper, we refer to the 2008-2014 period as current climate, and to the 2089-2095 period as future climate.

Out of predictions from those models, we use the vertical wind speed at 500 hPa (ω_{500}) and the Cloud Radiative Effect (CRE) decomposed in 3 components: Net, LW and SW. The simulated CRE includes contributions of both opaque and non-opaque clouds.

2.2.2 Lidar Simulator: COSP 1.4

On each model was plugged the COSP1.4 (CFMIP Observation Simulator Package) lidar simulator (Bodas-Salcedo et al., 2011), which reproduces synthetic lidar observations that would be measured by existing spaceborne lidars flying over the atmosphere predicted by the model (Chepfer

et al., 2008). Here, from COSP outputs we use the monthly gridded opaque cloud cover (Copaque) and altitude (Zopaque).

3 Relationship between Opaque cloud and Vertical air velocity in current observations

The distribution of ascending and subsiding air motions, according to vertical wind speed from reanalyses (Figure 1a), appears to drive the geographic patterns followed by the average altitude (Figure 1b) and cover (Figure 1c) of opaque clouds derived from spaceborne lidar observations (section 2.1). In ascending air motion (ω_{500}<0, red in Figure 1a), opaque clouds are high and abundant, generally Zopaque>3km (Figure 1b) and Copaque>40% (Figure 1c). This is the case over the InterTropical Convergence Zone (ITCZ), the mid-West Pacific Ocean and the warm pool, for instance. In subsiding air motion (ω_{500}> 0, blue in Figure 1a), opaque clouds are generally low and few, with Zopaque<3km (Figure 1b) and Copaque<40% (Figure 1c). However, many opaque (Copaque>60%) low altitude (Zopaque<1km) clouds are found in the edges of the West coast of America (Mexico and Peru), of Africa (Angola/Namibia) and of Australia, corresponding to stratocumulus regions. To better understand the relationship between the altitude and cover of opaque clouds and vertical air motions, we focus on how opaque clouds and ω_{500} vary together.

Figure 2 shows how the opaque cloud altitude, Zopaque, and the opaque cloud cover, Copaque, relate to the vertical velocity at 500 hPa, ω_{500}. These figures suggest the existence of two different regimes based on vertical velocity, linking cloud properties and dynamics in the Tropics. In the right regime, related to strong subsidence (ω_{500}>20 hPa/d, 38% of points), Zopaque is stable between 0 and 2 km, whatever the vertical wind speed at 500hPa (Figure 2a). Meanwhile, the mean Copaque increases slightly with subsidence speed (+6% from +25 to +75 hPa/d); dispersion is large for a given ω_{500} though. In the left regime, related to weak subsidence and convection (ω_{500} < 20 hPa/d, 62% of points), as ascendance gets stronger, both cover and altitude of opaque clouds

246 increase (Figs. 2a and b): Copaque increases on average by +17% between 20 and -75 hPa/day.
247 Zopaque goes from an average of 1.5km at +20 hPa/day (subsiding air motion), to 3.8km at -25
248 hPa/day (weak ascending air motion), up to a 5km average at -75 hPa/day (deep ascending air
249 motion). The Zopaque altitude is by definition lower than the top of the opaque cloud (section 2.1),
250 so opaque clouds probably extend higher than 5km. Strong ascending motion (<-50 hPa/day)
251 represent less than 10% of points of the tropical belt (PDF Figure 2a).

252 These results are consistent with Vaillant de Guélis et al. (2017a), and show that spaceborne
253 lidar observations and reanalysis suggest there is a clear relationship between atmospheric dynamics
254 (ω_{500}) in the Tropics and opaque cloud properties (Zopaque and Copaque). In the next section, we
255 evaluate how the 2 models CESM1 and IPSL-CM6 simulate patterns of ω_{500}, Zopaque and Copaque.

256 # 4 Relationship between Opaque cloud and Vertical air velocity in
257 simulations of current climate
258

259 ## 4.1 Geographic patterns of opaque cloud properties and dynamic regimes
260

261 Figs. 3a (CESM1) and b (IPSL-CM6) show that both models simulate geographic patterns of
262 ω_{500} similar to those from the reanalyses (black lines in Figs. 3a and 3b) in current climate conditions
263 (see also Figure S1 in Supplementary Information). Both models frequently simulate stronger
264 ascendance (ω_{500}<0, red 6 in Figs. 3c and 3d) North of the ITCZ, West of the Warm Pool and East of
265 the South Pacific Convergence Zone, weaker ascendance (ω_{500}<0, red 5) South of the ITCZ and across
266 the Warmpool, and stronger subsidence (blue 1) in the subsidence region of the South Equatorial
267 Pacific and in the North and South Atlantic. Both models tend to simulate ascendance instead of
268 subsidence at the southwest edges of subsidence-dominated areas (light salmon 4), for instance in
269 the South Pacific and West Indian Ocean. IPSL-CM6 simulates subsidence where ERA5 says
270 ascendance (cyan 3) between the subsidence zone of the Equatorial Pacific and the Warm pool.

CESM1 underestimates opaque cloud altitude on average almost everywhere by ≈0.5 km (Figure 3e) compared to observations (Figure 1b) and overestimates opaque cloud cover (+3.1 %, Figure 3g) almost everywhere except in stratocumulus regions. In contrast with CESM1, IPSL-CM6 overestimates Zopaque (+1.48km on average, Figure 3f) and Copaque (+7.7%, Figure 3h) almost everywhere except in the West part of the Equatorial Pacific (blue in the center of Figure 3f and h), which is consistent with the fact that IPSL-CM6 simulates subsidence instead of ascendance and increased subsidence in this region (cyan 3 and blue 1 in Figure 3d). Off the West coast of South America, both models underestimate stratocumulus cover (dark blue in Figure 3g and h), a well-known bias in climate models. Both models start to disagree further west, in the shallow cumulus region: CESM1 underestimates their cover, while IPSL-CM6 overestimates it.

4.2 Distributions of opaque cloud properties vs. dynamic regimes

We now analyze how both models simulate the relationships between cloud properties and ω_{500} in the current climate (Figure 4). The two regimes on each side on 20 hPa/d that were found in observations also appear in model simulations. CESM1 (Figure 4, left column) underestimates Zopaque (first row) in weak ascendance and subsidence (Figure 4a), and overestimates it in strong ascendance (ω_{500}<-50 hPa/d, Figure 4a) compared to observations (dotted black line with ±2 std). CESM1 (red line) put clouds at lower levels (below 1 km, PDF at right of the Figure 4a) than observations (grey area). Significant underestimates occur between 2 and 5 km, which is contributed from -50 to +25 hPa/day regimes, which are dominant (ω_{500} PDF, bottom left). IPSL-CM6 (right column) overestimates Zopaque significantly: >2km on average in left regime, and the overestimation is the largest near -25 hPa/d (Figure 4b) where most of ascending ω_{500} points are. The PDF (Figure 4b, right side) shows that IPSL-CM6 simulates more high opaque clouds (8-10km) and fewer very low opaque clouds (~1km) compared to observations. The CESM1 overestimate of Copaque (second row) increases with the ascendance speed (Figure 4c), while IPSL-CM6 overestimates Copaque for all ω_{500} (Figure 4d). In strong subsidence (right regime), only CESM1

overestimates the opaque cloud cover, but put too few thin clouds by half (Appendix, Figure S2). The effect dominates the tropical distribution of thin clouds cover (Appendix, Figure S3), consistently with the 'too few, too bright' problem (Nam et al., 2012). According to the PDF (right side of Figure 4c and d), CESM1 overestimates medium Copaque (20-40%) significantly and underestimates small Copaque (<20%), while IPSL-CM6 is mostly consistent with the PDF of observations (IPSL-CM6 overestimates a little Copaque below 35% and underestimates it above 35% in the PDF, Figure 4d, right side). So, CESM1 reproduces the relationship between Zopaque and ω_{500} better than IPSL-CM6, but IPSL-CM6 reproduces the global PDF of Copaque better than CESM1.

4.3 Distributions of cloud radiative effects vs. dynamic regimes

Using the same approach as Vaillant de Guélis et al., 2018, we found that opaque clouds contribute 87% (IPSL-CM6) and 78% (CESM1) of the current climate CRE, hence here we interpret CRE predictions through the properties of opaque clouds first. Both models overestimate the CRE_{LW} where they overestimate Zopaque and Copaque: in strong ascendance (ω_{500}<-50 hPa/d) for CESM1 (Figs. 4a 4c and 4e) and in ascendance for IPSL-CM6 (Figs. 4b, 4d and 4f). CESM1 underestimates the CRE_{LW} (Figure 4e) where it underestimates Zopaque, in subsidence and weak ascendance. This is consistent with higher opaque clouds producing a stronger greenhouse effect in the longwave. Both models overestimate the CRE_{SW} in ascendance (Figs. 4g and 4h), mainly due to overestimated Copaque at those regimes (Figs. 4c and 4d), CRE_{sw} not being sensitive to Zopaque. This is consistent with more opaque clouds producing a stronger albedo effect in the shortwave. Both models overestimate a lot the CRE_{net} compared to observations (dotted black lines in Figs. 4i and 4j), mostly due to their overestimate of CRE_{SW} caused by overestimated Copaque. This happens in all dynamic situations, and is especially notable in the left regime.

To sum up, Table 2 shows how model biases in CRE (evaluated against CERES measurements) correlate with model biases in cloud properties (evaluated against CALIPSO retrievals). For both models, biases in LW and SW CRE are strongly correlated with bias in Copaque. Biases in LW CRE are

also strongly correlated with bias on Zopaque. For both models, the bias in net CRE is correlated with the bias in Copaque, but not with the bias in Zopaque. Model bias on all CRE is linked to model bias on opaque cloud cover, while only model bias on LW CRE is linked to the bias on opaque cloud altitude (see Figure S4).

	Correlation between	Model Bias in LW CRE	Model bias in SW CRE	Model bias in total CRE
IPSL-CM6	Zopaque bias	0.59		-0.04
	Copaque bias	0.57	-0.71	-0.56
CESM1	Zopaque bias	0.76		-0.07
	Copaque bias	0.52	-0.69	-0.54

Table 2: Correlation coefficient between model biases in CRE (evaluated against CERES measurements) vs model bias in cloud property (evaluated against CALIPSO retrievals) calculated based on 2°x2° monthly mean values. All correlation coefficients are statistically significant at 99% confidence level. See Figure S4 in supplementary material.

CESM1 underestimates Zopaque (except in strong ascendance) and overestimates Copaque. Both effects lead to an underestimate of CRE_{LW}, an overestimate of CRE_{SW} and a CRE_{net} too negative compared to observations. The IPSL-CM6 CRE PDF is consistent with observations, but IPSL-CM6 locates opaque clouds much higher (>2km) than observations in ascendance (-50 hPa/d to 0 hPa/d), a situation that the model overestimates compared to reanalyses (ω_{500} PDF below Figure 6j). Since the model is able to simulate a correct total CRE, the strong error in Zopaque must be compensated by less visible, symmetrical errors in at least one other cloud property (e.g. opacity, cover). IPSL-CM6 overestimates the cover of opaque clouds (Figure 4d) and severely underestimates the cover of thin clouds (Figs. S2 and S3, Appendix). The relationships between cloud properties and CRE are shown in the Appendix for completeness (Figs. S5 and S6).

Let's see how CESM1 and IPSL-CM6 predict patterns of ω_{500}, Zopaque and Copaque in the future climate.

5 Relationship between Opaque cloud and Vertical air velocity in predictions of future climate

5.1 Changes in geographic patterns of opaque cloud properties and dynamic regimes

Figs. 5a (CESM1) and b (IPSL-CM6) show that geographic patterns of ω_{500} remain largely the same in the future. Both CESM1 and IPSL-CM6 predictions appear dominated by a weakening of upward motion in ascendance regions (red 5, Figure 5c and d) and a weakening of downward air motion in subsidence regions (blue 2, Figure 5c and d), i.e. both models predict a weakening of the Hadley/Walker circulation. CESM1 predicts that in a warmer climate opaque clouds will be lower (-2km, Figure 5e) in the Warm Pool and in the ITCZ but higher in the ascendance zone of the Southwest Pacific (+ 1km, Figure 5e) and in the subsidence zone of the East Equatorial Pacific (+2km, Figure 5e), and that there will be fewer of them almost everywhere (Figure 5g), except in the stratocumulus area (+20%, Figure 5g) at the west coast of South America. In a stark contrast, IPSL-CM6 predicts opaque clouds will rise almost everywhere, with the strongest rise (+3 km) in the subsidence region of the West Equatorial Pacific (Figure 5f). Exceptions are most of the North Atlantic, and parts of Southeast Pacific, where IPSL-CM6 predicts lower opaque clouds. It also predicts fewer opaque clouds in almost everywhere, with most notable exceptions in the center and South Pacific (Figure 5h). In ascendance regimes only, CESM1 predicts a very small average rise in Zopaque (+60m), while IPSL-CM6 predicts a much larger rise (+1.12km). This last value is consistent with the +700m rise that would occur following the Fixed Anvil Temperature hypothesis (Hartmann and Larson, 2002), considering an average +4°C increase in temperature between future and current climate (RCP8.5), and a loss of 6°C per km in the tropical troposphere.

In summary, both models agree on the weakening of the Hadley/Walker circulation dominating the predictions. Both models also agree on a strong rise of opaque clouds altitude in the

Equatorial Pacific subsidence region, and on a decrease of their altitude in the North Atlantic. They disagree on opaque cloud altitude evolution almost everywhere else.

5.2 Changes in distributions of cloud properties vs. dynamic regimes

We now examine how relationships between ω_{500} and Zopaque/Copaque evolve in the future. The two regimes that were found in observations and model simulations, on each side on 20 hPa/d (Section 4), also appear in future predictions (Figure 6, dashed vertical line).

The distribution changes shown in Figure 6, when coupled with the predicted changes in ω_{500}, help explain the maps of changes in cloud properties discussed in the last section. The changes in Zopaque in a given region can be explained by 1) a change in the Zopaque distribution for a given ω_{500}, i.e. a vertical move on the joint Zopaque-ω_{500} distribution, 2) a change in the ω_{500} distribution in the region, i.e. a horizontal move in the joint Zopaque-ω_{500} distribution, or 3) a combination of both. For instance, were ω_{500} to remain constant over all the Tropics, CESM1 predicts that Zopaque would rise in ascendance and would remain stable in subsidence (Figure 6a). However, CESM1's main prediction is the weakening of the Hadley/Walker circulation, i.e. that positive and negative ω_{500} will both mostly evolve towards zero. Since in regions dominated by strong subsidence (ω_{500} >20hPa/day), Zopaque distributions are stable with ω_{500} (right regime in Figure 4a and 6a), any Zopaque change will be driven by a change in its distribution (blue and red in the right regime of Figure 6a), leading to a rise in Zopaque in most weakening subsidence areas (blue 2 in Figure 5a). In such regions, the thermodynamic (joint Zopaque-ω_{500} distribution) changes have no effect on the Zopaque, instead the dynamic (ω_{500}) changes drive the Zopaque change. By contrast, in regions dominated by weak subsidence or ascendance (ω_{500} <20hPa/day), Zopaque distributions strongly depend on the average ω_{500}: Zopaque are distributed at higher altitudes for more negative ω_{500} in present and future simulations (left regime in Figure 4a and 6a). Hence, weakening ascendance would lead to a decrease in Zopaque in the future if the joint Zopaque-ω_{500} distribution remained constant. This relationship, however, does not remain constant: instead, it evolves towards higher

394 Zopaque for any $\omega_{500}<0$ (Figure 6a). Thus, regions of predicted weakened ascendance (red 5 in Figure
395 5c) will see a decrease in Zopaque if ω_{500} changes (dynamic) are more important than changes in the
396 joint Zopaque-ω_{500} distribution (thermodynamic). This is the case over the Warm Pool or the South
397 Pacific Convergence Zone (Figure 5e). In such regions, the evolution of Zopaque is dominated by
398 dynamic changes, and not by thermodynamic changes. Regions of predicted weakened ascendance
399 could see an increase in Zopaque if changes in the joint Zopaque-ω_{500} distribution are more
400 important than changes in the ω_{500} in the region. Such regions appear rare in Figure 5e.

401 In contrast with CESM1, the IPSL-CM6 joint Zopaque-ω_{500} distributions in current and future
402 climate (Figure 4b and 6b) are rather stable with ω_{500}, except in the ±15hPa/day range, where it
403 fluctuates wildly. Hence, changes in predicted ω_{500} (dynamic changes) have little influence on the
404 predicted Zopaque, except in regions where ω_{500} get close to or through the ±15hPa/day range: for
405 instance, over the edges of the central pacific equatorial area ω_{500} gets close enough to zero to
406 trigger a strong rise in Zopaque. These changes in Zopaque are driven by dynamic changes. Regions
407 of predicted weakened ascendance (red 5 in Figure 5d), as long as the average ω_{500} remain out of the
408 ±15hPa/day range, are instead affected by the change in joint Zopaque-ω_{500} distribution (Figure 6b),
409 which predicts a general rise, observable for instance over the warm pool. Such changes are driven
410 by thermodynamic changes. Thus, in IPSL-CM6 predictions, both dynamic and thermodynamic
411 changes lead to increases in Zopaque.

412 Regarding the opaque cloud cover (Figs. 6c and d), both models predict a decrease of Copaque
413 in average (-2.4% for CESM1 and -2.1% for IPSL-CM6). But, CESM1 predicts Copaque will decrease in
414 all regimes, most in ascendance and less in subsidence (Figure 6c), while IPSL-CM6 predicts an
415 increase of Copaque in ascendance and a decrease in subsidence (Figure 6d). So, for increasingly
416 negative ω_{500}, CESM1 and IPSL-CM6 agree on the evolution of Zopaque (they both make it rise) but
417 on the evolution of Copaque (they both make it decrease).

In summary, CESM1 predicts no change in Zopaque while IPSL-CM6 predicts a rise of opaque clouds for any fixed ω_{500}, but the general weakening of the vertical winds across the Tropics sometimes takes priority over this rise and leads to a decrease in Zopaque. Zopaque changes in CESM1 appear driven by dynamic changes everywhere. IPSL-CM6 changes of Zopaque appear mostly driven by thermodynamic changes, except in regions of weak ascendance and subsidence where dynamic changes dominate. What drives the Zopaque changes is thus dependent on the shape of the joint Zopaque-ω_{500} distribution in the model.

5.3 Changes in distributions of cloud radiative effect vs. dynamic regimes

Since we find the future change of clear-sky upwelling TOA flux is 5-12% of the change of the all-sky upwelling TOA flux in both models, we can suppose that the evolution of the CRE is mainly related to changes in clouds. Following again the Vaillant de Guélis et al. (2018) approach shows that opaque clouds still dominate the CRE in future climate conditions (87% for IPSL-CM6, 84% for CESM1), so we can again interpret the CRE changes in light of opaque cloud property changes.

The future CRE_{LW} will decrease in all regimes according to CESM1 (Figure 6e). This is consistent with its predicted decrease of Copaque (Figure 6c), but not with its predicted rise in Zopaque (Figure 6a). Thus the evolution of Copaque drives the evolution of the CRE_{LW} for CESM1. IPSL-CM6 predicts an increase of CRE_{LW} in moderate ascendance ($-50 < \omega_{500} < 0$ hPa/d, Figure 6f), consistent with its predicted increase of Zopaque and Copaque. IPSL-CM6 predicts a decrease of CRE_{LW} in subsidence, consistent with the predicted decrease in Copaque (Zopaque does not change). This decrease dominates the evolution of the CRE_{LW} PDF in IPSL-CM6 predictions (right side of Figure 6f).

The future CRE_{SW} will be weaker in all regimes according to CESM1 (Figure 6g), except in strong ascendance. This weakening is consistent with the decrease CESM1 predicts for Copaque, the main driver of CRE_{SW}. IPSL-CM6 predicts a stronger CRE_{SW} in ascendance (Figure 6h), consistent with the

increase predicted for Copaque (Figure 6d). The opposite is true in the right regime, where IPSL-CM6 predicts a weaker CRE_{SW}, linked to a decrease in Copaque.

The future CRE_{net} will change little overall according to the two models (Figs. 6i and 6j), especially in the most frequent regimes (-25hPa/d to 25hPa/d) which stay constant. In moderate to strong ascendance (ω_{500}<-25hPa/d), the future CRE_{net} will be more strongly negative according to both models. For CESM1, this is due to the decrease predicted for the CRE_{LW}, which in strong ascendance is not compensated by a decrease in CRE_{SW}. As shown above, in this case Copaque changes drive the evolution of the CRE_{LW}, hence the Copaque decrease predicted by CESM1 is responsible for the CRE_{net} change in strong ascendance (Figure 6i). For IPSL-CM6, the change is due to the stronger CRE_{SW}, driven by the increase predicted for Copaque. In moderate to strong subsidence (ω_{500}>25hPa/d), both models predict a weakening of the future CRE_{net}, linked to a weaker CRE_{SW} caused by a decrease Copaque. In the end, the small predicted CRE_{net} changes (in both subsidence and ascendance) are due to Copaque changes in both models.

In summary, in the future, in ascendance, CESM1 raises Zopaque (increase of CRE_{LW}, more warming) and decreases Copaque (decrease of CRE_{SW}, less cooling and decrease of CRE_{LW}, less warming). Since CESM1 actually predicts a CRE_{net} more negative (more cooling), only the effect of Copaque on the CRE_{LW} is consistent with this change, and Copaque changes drive the evolution of the CRE_{net} in CESM1. In the current climate, CESM1 overestimates Copaque (Figure 4c). It is therefore unclear whether the CRE_{net} changes predicted by CESM1 are reliable. In the future, IPSL-CM6 raises Zopaque (increase of CRE_{LW}, more warming) and increases Copaque (increase of CRE_{SW}, more cooling and increase of CRE_{LW}, more warming). Since IPSL-CM6 predicts a CRE_{net} slightly more negative (more cooling), again the Copaque changes drives the evolution of the CRE_{net} through its impact on the CRE_{SW}. In subsidence, there are no changes in the CRE_{net} for both models in the future.

6 Discussion of future changes and their origins

6.1 Overview of future changes in dynamic regimes

Figure 7 sums up how models simulate, in the current and future climate, opaque cloud distribution and CRE. Looking first at cloud properties, in current climate compared to observations, CESM1 underestimates Zopaque everywhere (most in subsidence) while IPSL-CM6 overestimates Zopaque everywhere (most in ascendance, Figure 7a). Both models overestimate the cover of opaque clouds (Figure 7b). In the future climate, CESM1 predicts an increase of Zopaque for $\omega_{500} < -5$ hPa/d and a decrease of Zopaque for $\omega_{500} > -5$ hPa/d, while IPSL-CM6 predicts an increase of Zopaque everywhere (Figure 7a). For Copaque, CESM1 predicts a decrease everywhere in the future, while IPSL-CM6 predicts a slight decrease for $\omega_{500}>-5$ hPa/d and an increase for $\omega_{500}<-5$ hPa/d (Figure 7b).

When considering the CRE_{LW} (Figure 7c), both models simulate it quite well in current climate in ascendance ($\omega_{500} < -5$ hPa/d) compared to observations, but they underestimate it elsewhere. In the future, both models predict a decrease of the CRE_{LW} everywhere, except in ascendance ($\omega_{500} < -5$ hPa/d) where IPSL-CM6 predicts an increase. Considering the CRE_{SW} (Figure 7d), in the current climate, both models overestimate the CRE_{SW} everywhere compared to observations. In the future, CESM1 predicts a weaker CRE_{SW} in all regimes, consistent with the predicted decrease in opaque cloud cover (Figure 7b). IPSL-CM6 predicts that in the future CRE_{SW} will strengthen for $\omega_{500} < -5$ hPa/d and will weaken elsewhere: consistent with more opaque clouds for $\omega_{500} < -5$ hPa/d, but not consistent with more opaque clouds for $\omega_{500} > -5$ hPa/d. Considering the CREnet (Figure 7e), both models overestimate it a lot compared to observations. In the future, CESM1 predicts a stronger CRE_{net} for $\omega_{500} < -5$ hPa/d but a weaker CRE_{net} elsewhere, while IPSL-CM6 predicts no change in overall CRE_{net} in any regime.

For CESM1, the changes in Copaque in all regimes dominate the future evolution of the CRE_{LW}, of the CRE_{SW}, and of the CRE_{net}. For IPSL-CM6, there are only very little changes in Copaque or CRE_{net}

in any regime. Most noticeable is the increase in Zopaque , but this increase is only strong enough to make the CRE_{LW} rise in ascendance (ω_{500} < -5 hPa/d).

The radiative biases of each model in current climate compared to observations stay relevant in the future, and the cloud property biases they come from become stronger. CESM1 simulates a CRE_{net} too negative in current climate compared to observations (PDF CRE_{net} to the right of Figure 6i), linked to an overestimation of Copaque (20-60%) and an underestimation of low Copaque (<20%). This mechanism stays valid in future predictions, but with a decrease of Copaque which leads to a decrease in the CRE_{LW} well compensated by the decrease of CRE_{SW}. IPSL-CM6 predicts in future conditions a strengthening of the CRE_{SW} in moderate ascendance (-50hPa/d < w500 < 0hPa/d), a situation that it overestimates in current climate compared to observations (Sect. 4.3). In these conditions, it also predicts a strong rise (+2km) in the altitude of opaque clouds, which were already too high in current climate compared to observations. Through an increase in CRE_{LW}, these changes help compensate the strengthening of CRE_{SW} and bring the CRE_{net} close to the one IPSL-CM6 simulates in current climate conditions.

6.2 Impact of dynamic vs. thermodynamic changes on cloud properties

Finally, we try to evaluate, for each variable, if the simulated changes are due to changes in the ω_{500} distribution alone (dynamic changes), or to changes in the relationship between the variable and ω_{500} (thermodynamic changes). To do this, we consider the following. The Zopaque PDF is equivalent to the product of the ω_{500} PDF and the joint Zopaque-ω_{500} distribution. Multiplying the current ω_{500} PDF by the future joint Zopaque-ω_{500} distribution yields the future Zopaque PDF attributable to the change in the joint Zopaque-ω_{500} distribution alone. Multiplying the future ω_{500} PDF by the current joint Zopaque-ω_{500} distribution yields the future Zopaque attributable to the change in the ω_{500} distribution alone (see Figure S7). Subtracting each of those PDFs to the PDF of Zopaque in current climate quantifies the change to the Zopaque PDF due to the change in either the ω_{500} distribution or the joint Zopaque-ω_{500} distribution. We applied this methodology to each cloud

property and radiative effect. The obtained numbers are reported in Table 3, which shows the total predicted change between PDFs of cloud property and radiative effect due (1) only to the change in the ω_{500} distribution, and (2) due only to the change in the relationship between ω_{500} and the considered variable. Table 3 suggests that overall, for most variables, the changes in the relationship between the dynamic conditions and the variable (thermodynamic changes) drive its change in the future climate, with the changes in ω_{500} (dynamic changes) being secondary. Exceptions are the opaque cloud cover, and SW and total CRE changes predicted by IPSL-CM6, which appear to be primarily driven by changes in the distribution of atmospheric dynamics. These are however the properties that change less between current and future climate conditions.

		Change in variable distribution	
		Due to change in ω_{500} only	Due to change in relationship only
CESM1	Zopaque	11%	**24%**
	Copaque	7%	**25%**
	CRE LW	11%	**23%**
	CRE SW	12%	**21%**
	CRE net	4%	**6%**
IPSL-CM6	Zopaque	11%	**57%**
	Copaque	**15%**	10%
	CRE LW	15%	**27%**
	CRE SW	**14%**	11%
	CRE net	**10%**	6%

Table 3: Change in the distribution of cloud properties and CRE due to changes in the ω_{500} distribution only, and due to the changes in the relationship between the property and the ω_{500} only (see methodology and Figure S7 in the Supplementary Information). The bold values are the largest correlation coefficient for each variable.

7 Summary and conclusions

This paper had three goals. To reach the first, we established the link between atmospheric circulation, opaque cloud properties (altitude and cover) and Cloud Radiative Effect, in present day climate based on 7 years of observation. Our second goal was to investigate the same link in present-day simulations from 2 climate models. We found that compared to observations CESM1 overestimates medium (40%) opaque cloud covers, and underestimates large (60-80%) and small (0-20%) opaque cloud covers. CESM1 also overestimates low opaque cloud altitude (<1 km). IPSL-CM6 overestimates opaque cloud cover (+7.7 % on average, PDF shifted to high values) and overestimates high opaque cloud altitude in the present climate. In both models, CRE_{LW} is driven by both Zopaque and Copaque while CRE_{SW} is only driven by Copaque, in agreement with Guzman et al. (2017) and Vaillant de Guélis et al. (2017b). The relationship between opaque cloud properties and atmospheric dynamics is well simulated in CESM1 in current climate compared to IPSL-CM6 simulations, but the distribution of medium Copaque (20-50%) is extremely different compared to observations. Most notably, IPSL-CM6 overestimates the amount of weak ascendance and, in this condition, significantly overestimates the Zopaque (+2km). This overestimation of Zopaque helps IPSL-CM6 balance other errors to get its predicted CRE_{net} close to observations. For CESM1, it is the Copaque ~ 40% and the CRE_{SW} that are overestimated, which lead to an overestimate of the CRE_{net}, especially in the left regime (ascendance and weak subsidence). Even though the climate sensitivity and cloud feedback amplitude are quite similar for both models and fall within the CMIP6 spread, each model simulates cloud properties in a very different way.

To reach our third goal, we examined how climate models simulate the evolution of cloud properties and atmospheric dynamics in the Tropics during the next century, according to the RCP8.5 scenario. Both models in future climate predict weaker ascendance and weaker subsidence motions in regions dominated by ascendance and subsidence in current climate, respectively, consistent with many previous studies (e.g. Vecchi and Soden, 2006; Su et al., 2014). CESM1 in the future predicts

559 more medium opaque clouds (40%) but less extreme values (0-20% and 60-80%). It also predicts that
560 the PDF of Zopaque shift down a little in the future. IPSL-CM6, in the future, predicts a slight
561 decrease in average (-2.1%, Figure 5h) but significantly higher (+1.84km) opaque clouds almost
562 everywhere in the Tropics. The PDF of high Zopaque shifted by +2 km while the PDF of Copaque
563 remains stable in the future. Both models predict very little change in the mean net CRE in the future
564 on average. Small but noticeable changes in the net CRE (in relatively strong ascendance or
565 subsidence) can be explained by predicted changes in Copaque for both models, with changes in
566 cloud altitude having little influence. Even the very strong rise in Zopaque predicted by IPSL-CM6 in a
567 regime it generates too frequently (-50hPa/d<w_{500}<-25hPa/day) has no significant impact on the
568 evolution of the CRE_{net}. IPSL-CM6 strongly overestimates Zopaque in current climate compared to
569 observations in the same regime.

570 Our results show that even though the dynamic distribution (i.e. the ω_{500}) is the main influence
571 on model biases in ascendance in current climate conditions, changes in thermodynamic effects (e.g.
572 the temperature) are instead responsible for most of predicted changes in cloud properties and CRE.
573 This is true overall in both models for the altitude of attenuation of opaque clouds, and thus for their
574 vertical distribution. These conclusions change depending on the model and the location: in CESM1,
575 changes in the altitude of attenuation appear driven by changes in dynamic conditions in regions
576 dominated by ascendance and weak subsidence, and driven by changes in thermodynamic conditions
577 in regions dominated by strong subsidence. These results agree well with those from Xu and Cheng,
578 2016 who showed that, in weak subsidence, dynamic changes have a strong impact on cloud
579 feedback while thermodynamic changes have a strong impact on cloud feedback in moderate-to-
580 strong subsidence and strong convection. We find the opposite true in IPSL-CM6, due to the strong
581 differences in the shape of the joint Zopaque-ω_{500} distribution in both models.

582 In the end, we find that the variables affected by model biases in current climate conditions
583 change significantly in future climate condition, in a way that affect the CRE and cloud feedbacks. Our

results suggest that the representation in each model of opaque cloud properties in the current climate, including its relationship with atmospheric dynamics, has a strong impact on the model cloud feedback predictions. In the future, we hope to be able to leverage GCM simulations with high temporal resolution to investigate the impact that short-timescales processes can have on the relationship between cloud properties and their possible feedbacks.

Acknowledgments

The authors acknowledge J. Kay for providing the CESM1 simulations. The authors thank T. Vaillant de Guélis, P. Raberanto, M. Chiriaco and D. Bouniol for constructive discussions. Thanks are due to CNES/CNRS for contributing to the funding of this work, and to NASA/CNES and ClimServ/AERIS for providing CALIPSO data. We acknowledge the World Climate Research Program's Working Group on Coupled Modelling, responsible for CMIP. Finally, we thank the anonymous reviewers for useful comments and suggestions that helped improve the paper.

Data availability

CALIPSO-GOCCP observations data are available on https://climserv.ipsl.polytechnique.fr/cfmip-obs/Calipso_goccp.html . ERA5 reanalyses data are available on https://cds.climate.copernicus.eu/cdsapp#!/dataset/reanalysis-era5-pressure-levels-monthly-means?tab=form. All data that we use in this paper are available here: https://doi.org/10.14768/e91cc5fa-bcde-435c-b40f-65c93daae7d2

Figures

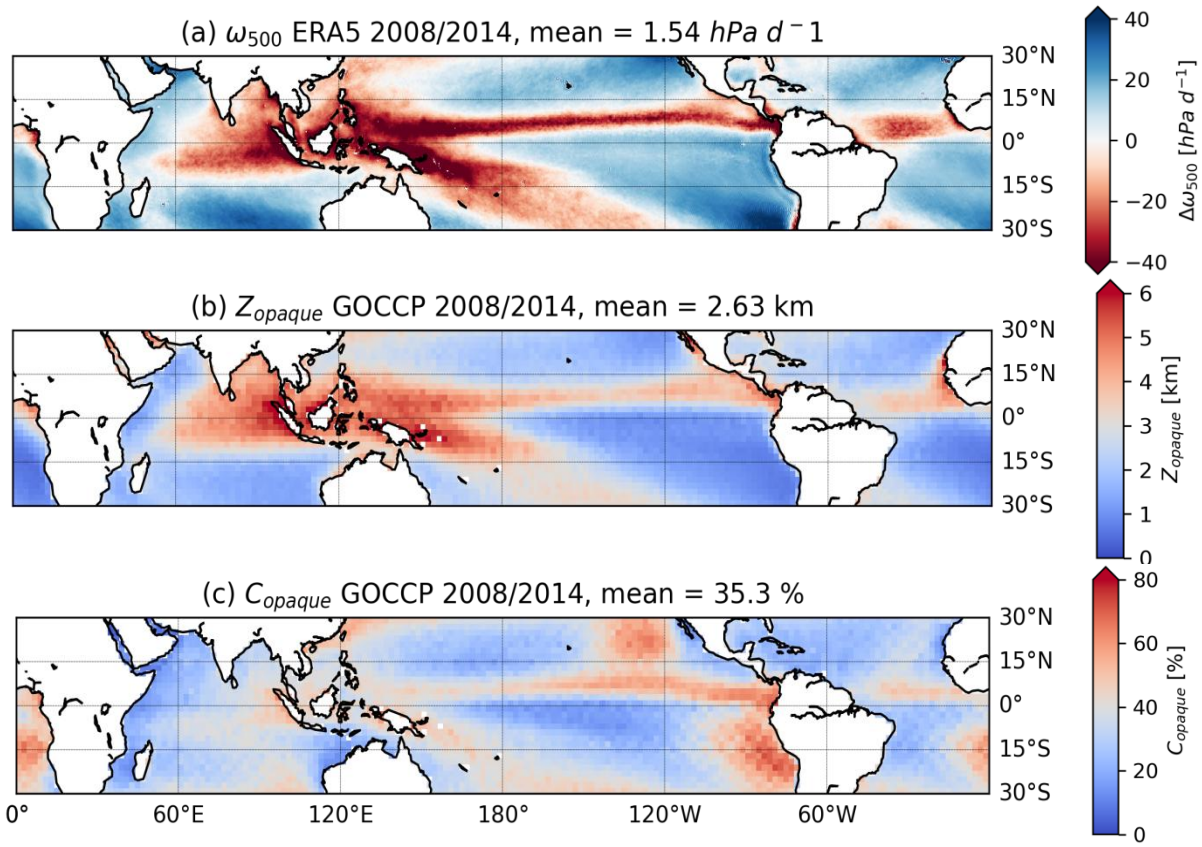

Figure 1: Maps of (a) vertical velocity at the 500 hPa level (ω_{500}) according to ERA5 reanalysis, (b) Zopaque and (c) Copaque according to CALIPSO GOCCP observations. Red represents ascending regions (ω_{500}<0), high Zopaque (Zopaque>3km) and large Copaque (Copaque>40%). Blue represents descending regions (ω_{500}>0), low Zopaque (Zopaque<3km) and small Copaque (Copaque<40%). Tropics [30°S-30°N] multi-annual mean averaged over the 2008-2014 period.

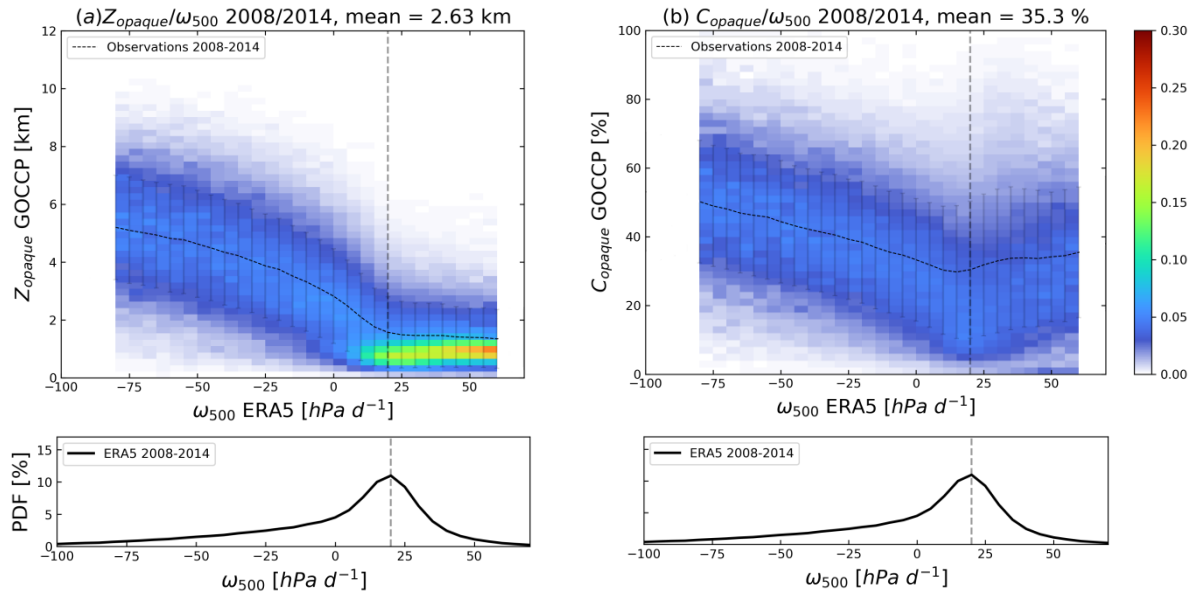

Figure 2: Normalized histogram showing the distribution of (a) Zopaque [km] and the vertical velocity at 500 hPa, ω_{500} [hPa/d], and (b) Copaque [%] and ω_{500} [hPa/d] considering values from all year monthly mean values over a 2°x2° grid [30°S-30°N], ocean only, for the 2008-2014 period combined with the probability distribution of monthly ω_{500} [hPa/d] over the 2008-2014 period. Zopaque and Copaque come from CALIPSO GOCCP observations, ω_{500} from ERA5 reanalysis. The dotted vertical line represents ω_{500}= +20 hPa/d. The dotted black curve represents the distribution over the 2008-2014 period according to GOCCP observations. To normalize, we divide Zopaque (Copaque) occurrences along the y-axis by the total number of occurrences in each ω_{500} bin. Hence, the sum of the normalized occurrences of Zopaque (Copaque) for a given ω_{500} is 1. ω_{500} ranges containing less than 2000 absolute occurrences are masked (white).

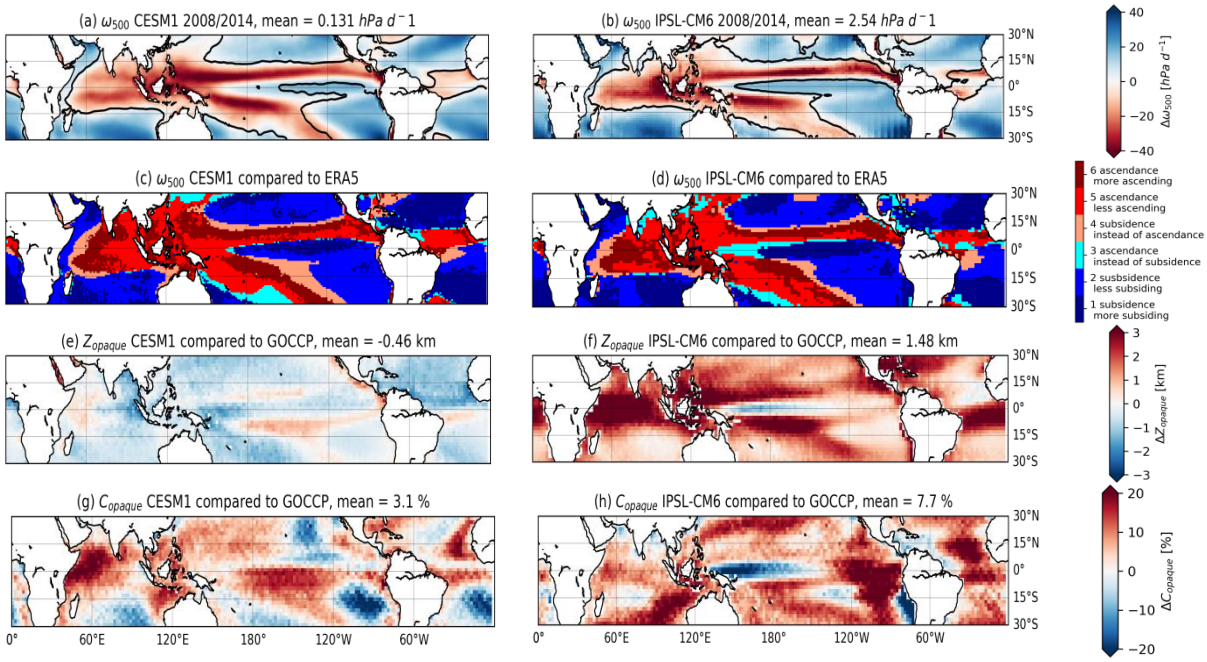

625

626 **Figure 3: Maps of (a and b) vertical velocity at 500 hPa (ω_{500}) from climate models in current climate. Maps of**
627 **differences between models and observations (c and d) vertical velocity at 500 hPa (ω_{500}), (e) and (f) opaque cloud**
628 **altitude (Zopaque) and (g) and (h) opaque cloud cover (Copaque). Left column refers to the CESM1 model and the right**
629 **column to the IPSL-CM6 model. Observations of Copaque and Zopaque are from CALIPSO-GOCCP, and ω_{500} from ERA-5**
630 **reanalyses. Black lines in a and b show the ω_{500} = 0 hPa/d isocontour in ERA5 reanalyses. All data averaged over the**
631 **2008-2014 period.**

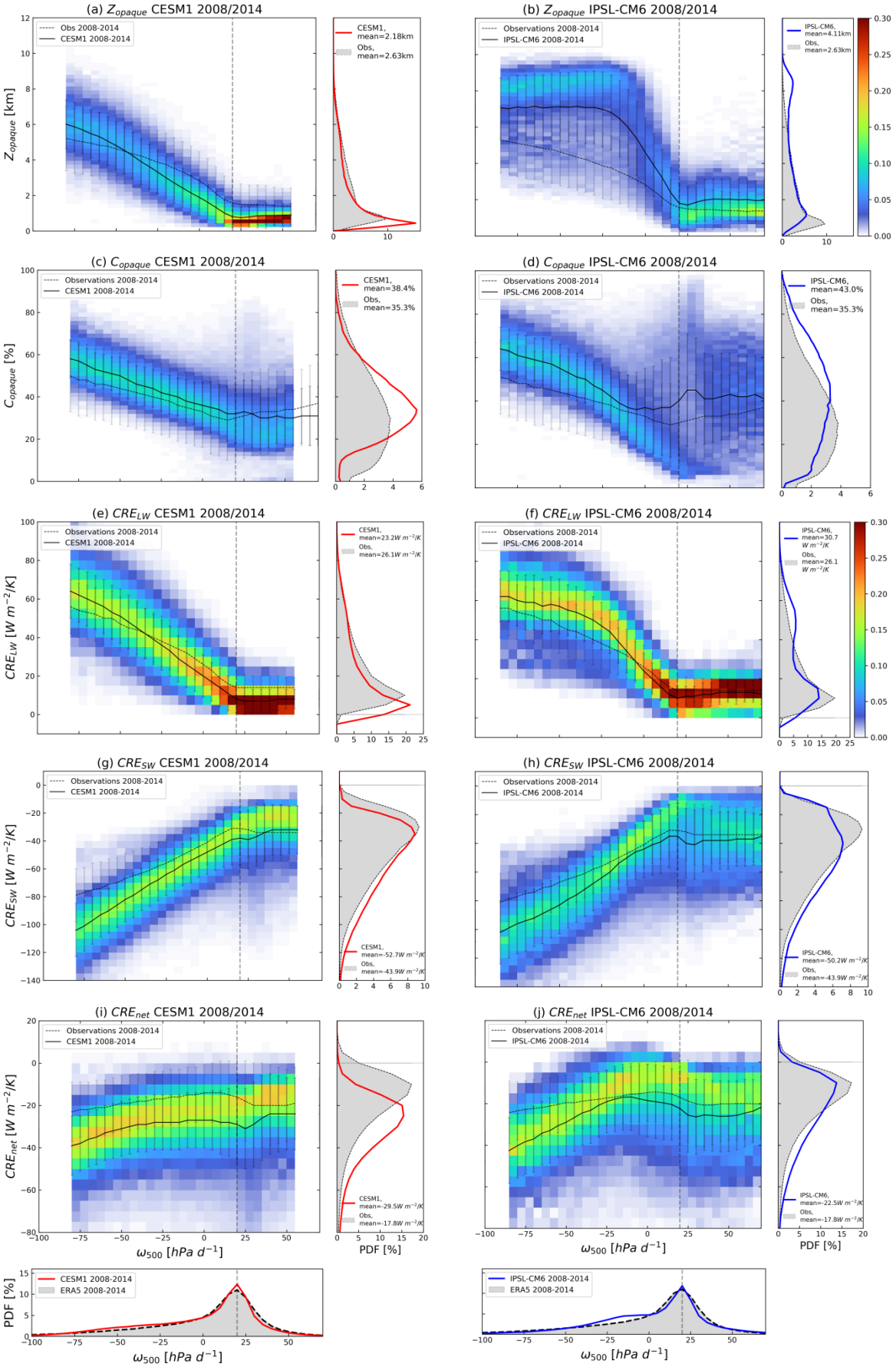
(a) Z_{opaque} CESM1 2008/2014
Obs 2008-2014
CESM1 2008-2014
Z_{opaque} [km]
CESM1, mean=2.18km
Obs, mean=2.63km
(b) Z_{opaque} IPSL-CM6 2008/2014
Observations 2008-2014
IPSL-CM6 2008-2014
IPSL-CM6, mean=4.11km
Obs, mean=2.63km
(c) C_{opaque} CESM1 2008/2014
Observations 2008-2014
CESM1 2008-2014
C_{opaque} [%]
CESM1, mean=38.4%
Obs, mean=35.3%
(d) C_{opaque} IPSL-CM6 2008/2014
Observations 2008-2014
IPSL-CM6 2008-2014
IPSL-CM6, mean=43.0%
Obs, mean=35.3%
(e) CRE_{LW} CESM1 2008/2014
Observations 2008-2014
CESM1 2008-2014
CRE_{LW} [$W\ m^{-2}/K$]
CESM1, mean=23.2$W\ m^{-2}/K$
Obs, mean=26.1$W\ m^{-2}/K$
(f) CRE_{LW} IPSL-CM6 2008/2014
Observations 2008-2014
IPSL-CM6 2008-2014
IPSL-CM6, mean=30.7 $W\ m^{-2}/K$
Obs, mean=26.1 $W\ m^{-2}/K$
(g) CRE_{SW} CESM1 2008/2014
Observations 2008-2014
CESM1 2008-2014
CRE_{SW} [$W\ m^{-2}/K$]
CESM1, mean=-52.7$W\ m^{-2}/K$
Obs, mean=-43.9$W\ m^{-2}/K$
(h) CRE_{SW} IPSL-CM6 2008/2014
Observations 2008-2014
IPSL-CM6 2008-2014
IPSL-CM6, mean=-50.2$W\ m^{-2}/K$
Obs, mean=-43.9$W\ m^{-2}/K$
(i) CRE_{net} CESM1 2008/2014
Observations 2008-2014
CESM1 2008-2014
CRE_{net} [$W\ m^{-2}/K$]
CESM1, mean=-29.5$W\ m^{-2}/K$
Obs, mean=-17.8$W\ m^{-2}/K$
ω_{500} [$hPa\ d^{-1}$]
PDF [%]
(j) CRE_{net} IPSL-CM6 2008/2014
Observations 2008-2014
IPSL-CM6 2008-2014
IPSL-CM6, mean=-22.5$W\ m^{-2}/K$
Obs, mean=-17.8$W\ m^{-2}/K$
ω_{500} [$hPa\ d^{-1}$]
PDF [%]
PDF [%]
CESM1 2008-2014
ERA5 2008-2014
ω_{500} [$hPa\ d^{-1}$]
IPSL-CM6 2008-2014
ERA5 2008-2014
ω_{500} [$hPa\ d^{-1}$]

Figure 4: Normalized histogram showing the distribution of (a and b) Zopaque [km], (c and d) Copaque [%], (e and f) CRE_{LW} [W/m²/K], (g and h) CRE_{SW} [W/m²/K] and (i and j) CRE_{net} [W/m²/K] and the PDF of the vertical velocity at 500 hPa, ω_{500} [hPa/d] in the Tropics [30°N-30°S], ocean only. The CESM1 model is in left column (red curves) and the IPSL-CM6 model in the right column (blue curves). ω_{500} ranges containing less than 2000 absolute occurrences for CESM1 and less than 1000 absolute occurrences for IPSL-CM6 are masked (white). The dotted black curve represents, for each variable, the distribution over the 2008-2014 period according to GOCCP observations and CERES observations and the black curve represents the distribution over the 2008-2014 period according to CESM1 and IPSL-CM6 simulations. The error bars show the ± 2 standard deviation of the 7-years means. PDF of monthly (a and b) Zopaque, (c and d) Copaque, (e and f) CRE_{LW}, (g and h) CRE_{SW} and (i and j) CRE_{net} to the right of each normalized histogram. PDFs of monthly ω_{500} under normalized histograms of CRE_{net}. The grey shadows represent the distribution over the 2008-2014 periods according to GOCCP observations (cloud properties), CERES observations (CRE) and ERA5 reanalysis (ω_{500}).

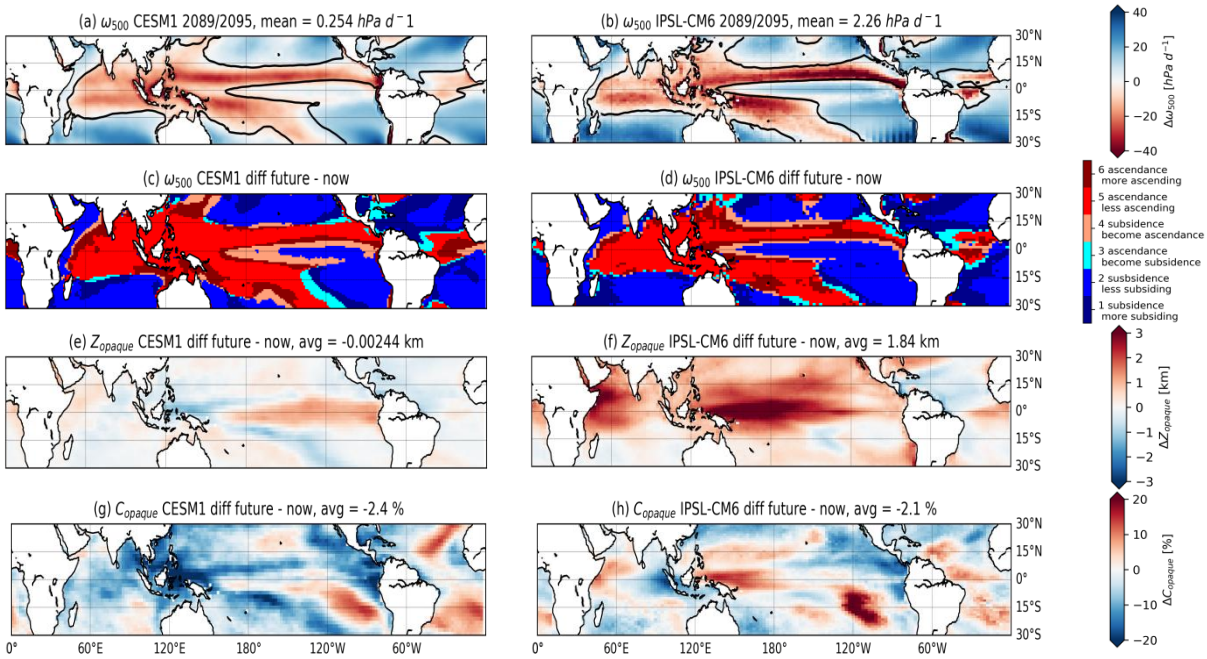

Figure 5: Maps of (a and b) vertical velocity at 500 hPa (ω_{500}) from climate models in future climate. Black lines in a and b show the ω_{500} = 0 hPa/d isocontour in present climate conditions. Maps of differences between future (2089-2095) and current (2008-2014) climate previsions of (c, d) vertical velocity at 500 hPa (ω_{500}), (e, f) opaque cloud altitude (Zopaque) and (g, h) opaque cloud cover (Copaque) in CESM1 (left column) and IPSL-CM6 (right column). Current climate is the reference.

651

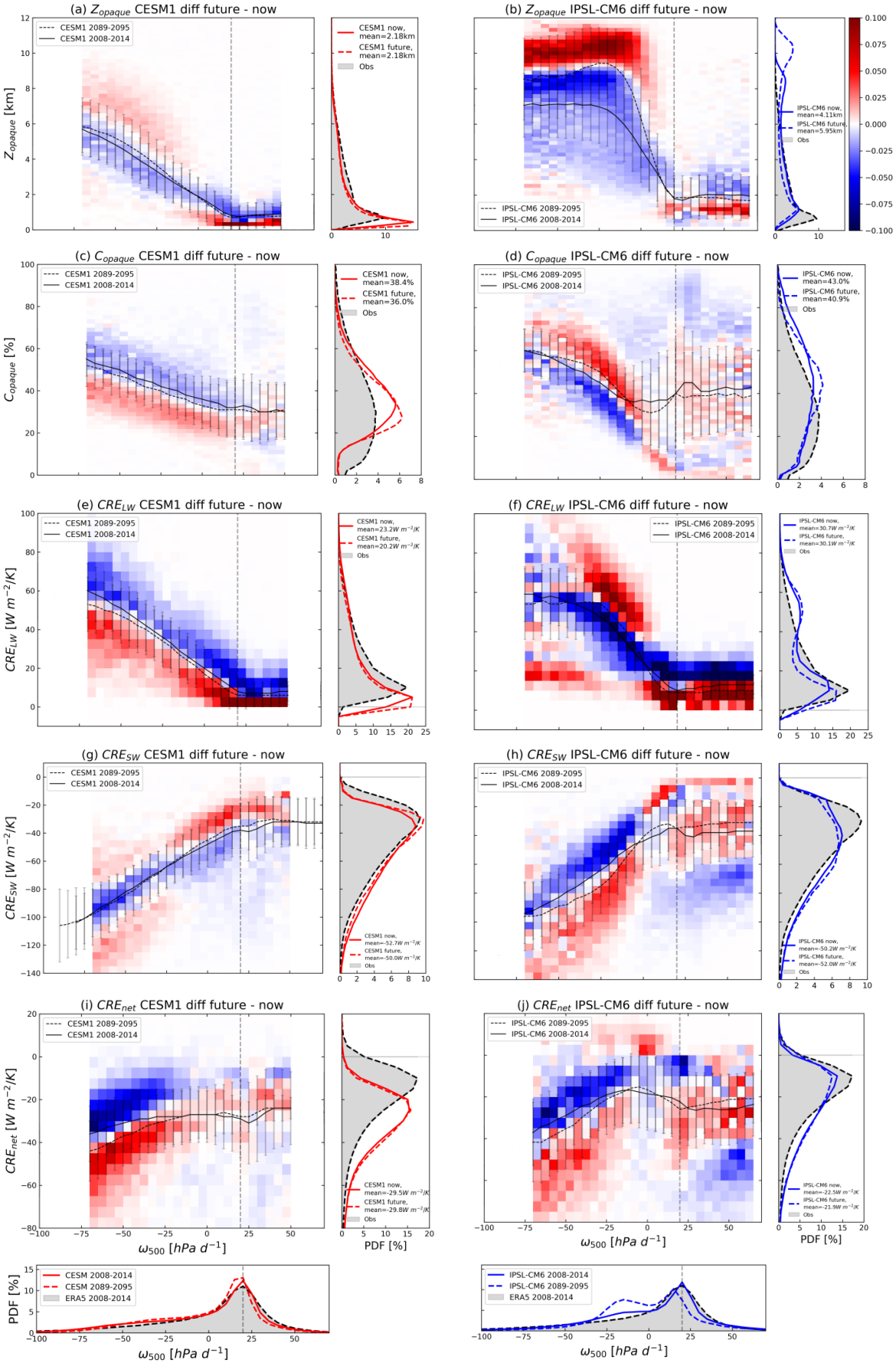
(a) Z_{opaque} CESM1 diff future - now
(b) Z_{opaque} IPSL-CM6 diff future - now
(c) C_{opaque} CESM1 diff future - now
(d) C_{opaque} IPSL-CM6 diff future - now
(e) CRE_{LW} CESM1 diff future - now
(f) CRE_{LW} IPSL-CM6 diff future - now
(g) CRE_{SW} CESM1 diff future - now
(h) CRE_{SW} IPSL-CM6 diff future - now
(i) CRE_{net} CESM1 diff future - now
(j) CRE_{net} IPSL-CM6 diff future - now
Z_{opaque} [km]
C_{opaque} [%]
CRE_{LW} [$W\ m^{-2}/K$]
CRE_{SW} [$W\ m^{-2}/K$]
CRE_{net} [$W\ m^{-2}/K$]
ω_{500} [$hPa\ d^{-1}$]
PDF [%]
CESM1 2089-2095
CESM1 2008-2014
CESM1 now, mean=2.18km
CESM1 future, mean=2.18km
IPSL-CM6 2089-2095
IPSL-CM6 2008-2014
IPSL-CM6 now, mean=4.11km
IPSL-CM6 future, mean=5.95km
CESM1 now, mean=38.4%
CESM1 future, mean=36.0%
IPSL-CM6 now, mean=43.0%
IPSL-CM6 future, mean=40.9%
Obs
CESM 2008-2014
CESM 2089-2095
ERA5 2008-2014
IPSL-CM6 2008-2014
IPSL-CM6 2089-2095
ERA5 2008-2014

Figure 6: Differences between future and current normalized histograms of (a and b) Zopaque [m], (c and d) Copaque [%], (e and f) CRE_{LW} [W/m²/K], (g and h) CRE_{SW} [W/m²/K] and (i and j) CRE_{net} [W/m²/K] and the PDF of the vertical velocity at 500 hPa, ω_{500} [hPa/d] in the Tropics [30°N-30°S], ocean only. The CESM model [2089-2095 / 2008-2014] is in left column (red curves) and the IPSL model [2089-2095 / 2008-2014] in the right column (blue curves). ω_{500} ranges containing less than 5000 absolute occurrences for CESM1 and less than 2000 absolute occurrences for IPSL-CM6 are masked (white). PDFs of monthly (a and b) Zopaque [hPa/d], (c and d) Copaque, (e and f) CRE_{LW}, (g and h) CRE_{SW} and (i and j) CRE_{net} to the right of each normalized histogram. The last row shows PDFs of monthly ω_{500}. Grey shadows represent the distributions of cloud properties according to GOCCP observations, of CRE according to and CERES observations (panels a-j) and the ω_{500} distribution from ERA5 reanalysis (w500 distribution, bottom) over the 2008-2014 period. Full curves represent the 2008-2014 period and dotted curves represent the 2089-2095 period.

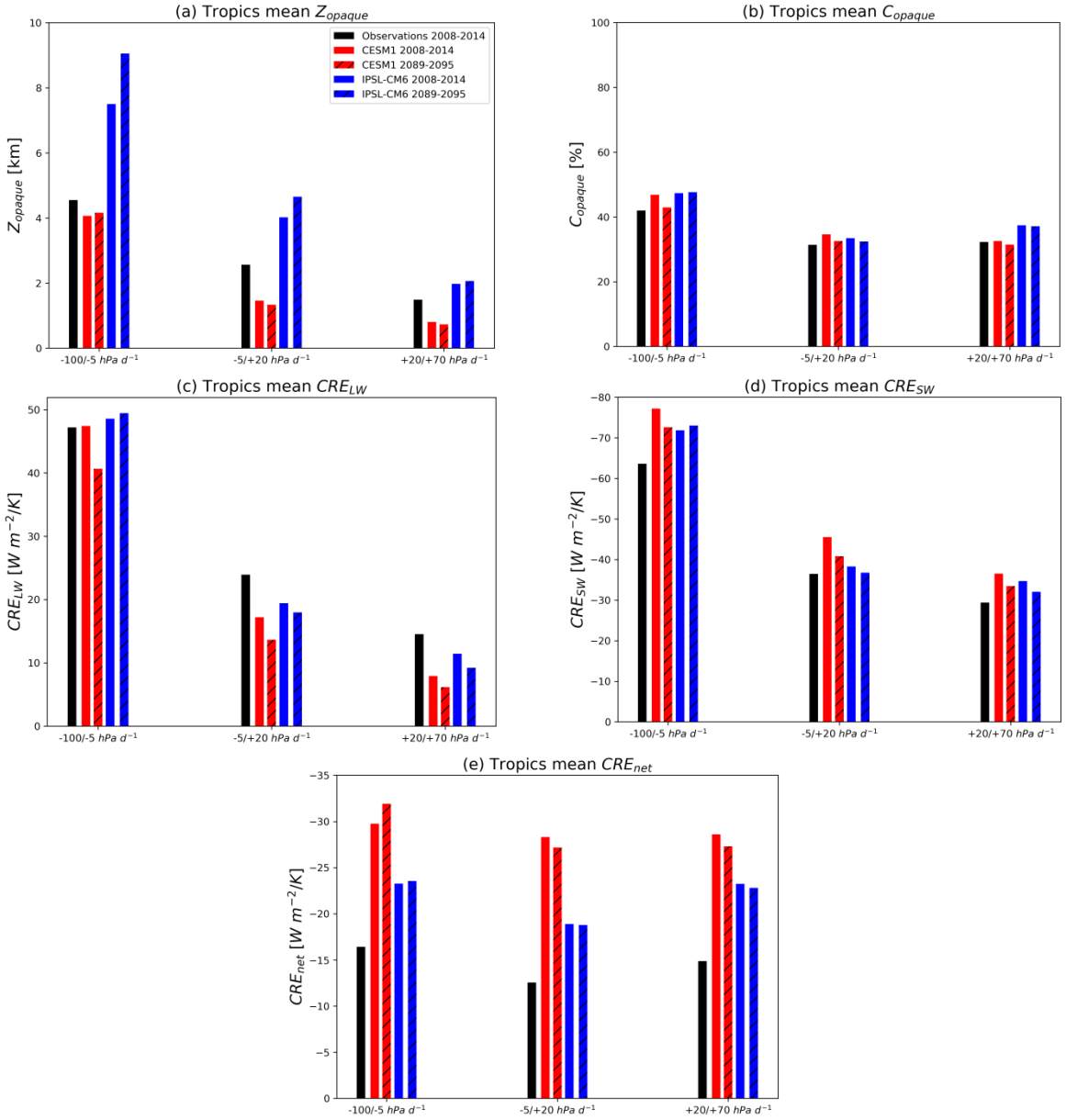

Figure 7: Mean values of (a) Zopaque, (b) Copaque, (c) CRELW, (d) CRESW and (e) CREnet over ω_{500}=+20/+70 hPa/d (right of each plot), ω_{500}=-5/+20 hPa/d (center of each plot) and ω_{500}=-100/-5 hPa/d (left of each plot) in the Tropics [30°S-30°N], ocean only. Observations (black) of Zopaque and Copaque are from CALIPSO-GOCCP (2008-2014) and observations of CREs are from CERES-EBAF (2008-2014). Simulations are from CESM (red) and IPSL-CM6 (blue) averaged over the 2008-2014 period (no pattern) and over the 2089-2095 period (dashed pattern).

Bibliography

- Aumont O., C. Ethe, A. Tagliabue, L. Bopp, M. Gehlen, 2015: Pisces-v2: an ocean biogeochemical model for carbon and ecosystem studies. *Geosci. Model Dev. Discuss.,* **8**, 1375–1509. https://doi.org/10.5194/gmdd-8-1375-2015
- Birner, T., 2010: Recent widening of the tropical belt from global tropopause statistics: Sensitivities. *J. Geophys. Res.*, **115**, D23109, https://doi.org/10.1029/2010JD014664.
- Bodas-Salcedo, A., and Coauthors, 2011: COSP: Satellite simulation software for model assessment. *Bull. Amer. Meteor. Soc.*, **92**, 1023–1043, https://doi.org/10.1175/2011BAMS2856.1.
- Bony, S. and J.-L. Dufresne, 2005: Marine boundary layer clouds at the heart of tropical cloud feedback uncertainties in climate models. *Geophys. Res. Lett.*, **32**, L20806, https://doi.org/10.1029/2005GL023851
- Bony, S., J.-L. Dufresne, H. Le Treut, J.-J. Morcrette, and C. Senior, 2004: On dynamic and thermodynamic components of cloud changes. *Climate Dynamics*, **22**, 71–86, https://doi.org/10.1007/s00382-003-0369-6.
- Bony, S., and Coauthors, 2006: How Well Do We Understand and Evaluate Climate Change Feedback Processes? *Journal of Climate*, **19**, 3445–3482, https://doi.org/10.1175/JCLI3819.1.
- Bony, S., G. Bellon, D. Klocke, S. Sherwood, S. Fermepin, and S. Denvil, 2013: Robust direct effect of carbon dioxide on tropical circulation and regional precipitation. *Nature Geosci*, **6**, 447–451, https://doi.org/10.1038/ngeo1799.
- Boucher, O., D. Randall, P. Artaxo, C. Bretherton, G. Feingold, P. Forster, V.-M. Kerminen, Y. Kondo, H. Liao, U. Lohmann, P. Rasch, S.K. Satheesh, S. Sherwood, B. Stevens, and X.Y. Zhang, 2013: Clouds and aerosols. In Climate Change 2013: The Physical Science Basis. Contribution of Working Group I to the Fifth Assessment Report of the Intergovernmental Panel on Climate Change. T.F. Stocker, D. Qin, G.-K. Plattner, M. Tignor, S.K. Allen, J. Doschung, A. Nauels, Y. Xia, V. Bex, and P.M. Midgley, Eds. Cambridge University Press, pp. 571-657, . https://doi:10.1017/CBO9781107415324.016.
- Boucher, O., Servonnat, J., Albright, A. L., Aumont, O., Balkanski, Y., Bastrikov, V., et al. (2020). Presentation and evaluation of the IPSL-CM6A-LR climate model. Journal of Advances in Modeling Earth Systems, 12, e2019MS002010. https://doi.org/10.1029/2019MS002010
- Caldwell, P. M., M. D. Zelinka, K. E. Taylor, and K. Marvel, 2016: Quantifying the Sources of Intermodel Spread in Equilibrium Climate Sensitivity. *J. Climate*, **29**, 513–524, https://doi.org/10.1175/JCLI-D-15-0352.1.
- Ceppi, P., F. Brient, M. D. Zelinka, and D. L. Hartmann, 2017: Cloud feedback mechanisms and their representation in global climate models: Cloud feedback mechanisms and their representation in GCMs. *WIREs Clim Change*, **8**, e465, https://doi.org/10.1002/wcc.465.
- Cesana, G., and H. Chepfer, 2012: How well do climate models simulate cloud vertical structure? A comparison between CALIPSO-GOCCP satellite observations and CMIP5 models. *Geophys. Res. Lett.*, **39**, 2012GL053153, https://doi.org/10.1029/2012GL053153.

- Cesana, G., Del Genio, A. D., and Chepfer, H. , 2019: The Cumulus And Stratocumulus CloudSat-CALIPSO Dataset (CASCCAD), *Earth Syst. Sci. Data*, **11**, 1745–1764, https://doi.org/10.5194/essd-11-1745-2019
- Cess, R. D., 1975: Global climate change: an investigation of atmospheric feedback mechanisms. *Tellus*, **27**, 193–198, https://doi.org/10.1111/j.2153-3490.1975.tb01672.x.
- Cess, R. D., Robert & Potter, Gerald & Blanchet, Jean-Pierre & Boer, G & Ghan, Steven & Kiehl, Jeffrey & Treut, H & Li, Z & Liang, X & Mitchell, J. & Morcrette, Jean-Jacques & Randall, D & Riches, M & Roeckner, E & Schlese, U & Slingo, A & Taylor, K & Washington, Warren & Wetherald, R & Yagai, I. , 1989: Interpretation of Cloud-Climate Feedback as Produced by 14 Atmospheric General Circulation Models. *Science* (New York, N.Y.). 245. 513-6. https://doi.org/10.1126/science.245.4917.513.
- Cess, R. D., M. H. Zhang W. J. Ingram G. L. Potter V. Alekseev H. W. Barker E. Cohen-Solal R. A. Colman D. A. Dazlich A. D. Del Genio M. R. Dix V. Dymnikov M. Esch L. D. Fowler J. R. Fraser V. Galin W. L. Gates J. J. Hack J. T. Kiehl H. Le Treut K. K.-W. Lo B. J. McAvaney V. P. Meleshko J.-J. Morcrette D. A. Randall E. Roeckner J.-F. Royer M. E. Schlesinger P. V. Sporyshev B. Timbal E. M. Volodin K. E. Taylor W. Wang R. T. Wetherald, 1996: Cloud feedback in atmospheric general circulation models: An update, *J. Geophys. Res.*, **101**(D8), 12791– 12794. https://doi.org/10.1029/96JD00822.
- Chepfer, H., S. Bony, D. Winker, M. Chiriaco, J.-L. Dufresne, and G. Sèze, 2008: Use of CALIPSO lidar observations to evaluate the cloudiness simulat*ed by a climate mod*el**.** *Geophys. Res. Lett.*, **35**, L15704, https://doi.org/10.1029/2008GL034207.
- Chepfer, H., S. Bony, D. Winker, G. Cesana, J. L. Dufresne, P. Minnis, C. J. Stubenrauch, and S. Zeng, 2010: The GCM-Oriented CALIPSO Cloud Product (CALIPSO-GOCCP). *J. Geophys. Res.*, **115**, D00H16, https://doi.org/10.1029/2009JD012251.
- Chepfer, H., G. Cesana, D. Winker, B. Getzewich, M. Vaughan, and Z. Liu, 2013: Comparison of Two Different Cloud Climatologies Derived from CALIOP-Attenuated Backscattered Measurements (Level 1): The CALIPSO-ST and the CALIPSO-GOCCP. *Journal of Atmospheric and Oceanic Technology*, **30**, 725–744, https://doi.org/10.1175/JTECH-D-12-00057.1.
- Chepfer, H., V. Noel, D. Winker, and M. Chiriaco, 2014: Where and when will we observe cloud changes due to climate warming? *Geophys. Res. Lett.*, **41**, 8387–8395, https://doi.org/10.1002/2014GL061792.
- Chepfer, H., V. Noel, M. Chiriaco, B. Wielicki, D. Winker, N. Loeb, and R. Wood, 2018: The Potential of a Multidecade Spaceborne Lidar Record to Constrain Cloud Feedback. *J. Geophys. Res. Atmos.*, **123**, 5433–5454, https://doi.org/10.1002/2017JD027742.
- Chepfer, H., H. Brogniez, and V. Noel, 2019: Diurnal variations of cloud and relative humidity profiles across the tropics. *Sci Rep*, **9**, 16045, https://doi.org/10.1038/s41598-019-52437-6.
- Chou, C., and J. D. Neelin, 2004: Mechanisms of Global Warming Impacts on Regional Tropical Precipitation. *JOURNAL OF CLIMATE*, **17**, 14. https://doi.org/10.1175/1520-0442(2004)017%3C2688:MOGWIO%3E2.0.CO;2
- Colman, R., 2003: A comparison of climate feedbacks in general circulation models. *Climate Dynamics,* **20**, 865–873. https://doi.org/10.1007/s00382-003-0310-z
- Cooper, R. N., J. T. Houghton, J. J. McCarthy, and B. Metz, 2002: Climate Change 2001: The Scientific Basis. *Foreign Affairs*, **81**, 208, https://doi.org/10.2307/20033020.

- Davis, S. M., and K. H. Rosenlof, 2012: A Multidiagnostic Intercomparison of Tropical-Width Time Series Using Reanalyses and Satellite Observations. *Journal of Climate*, **25**, 1061–1078, https://doi.org/10.1175/JCLI-D-11-00127.1.

- Dupont, J.-C., and Haeffelin, M. ,2008: Observed instantaneous cirrus radiative effect on surface-level shortwave and longwave irradiances, *J. Geophys. Res.*, **113**, D21202, https://doi:10.1029/2008JD009838.

- Eyring, V., Bony, S., Meehl, G. A., Senior, C. A., Stevens, B., Stouffer, R. J., & Taylor, K. E. (2016). Overview of the Coupled Model Intercomparison Project Phase 6 (CMIP6) experimental design and organization. *Geosci. Model Dev.*, 22., https://doi.org/10.5194/gmd-9-1937-2016.

- Frey, W. R., A. L. Morrison, J. E. Kay, R. Guzman, and H. Chepfer, 2018: The Combined Influence of Observed Southern Ocean Clouds and Sea Ice on Top-of-Atmosphere Albedo. *J. Geophys. Res. Atmos.*, **123**, 4461–4475, https://doi.org/10.1029/2018JD028505.

- Gettelman, A., Hannay, C., Bacmeister, J. T., Neale, R. B., Pendergrass, A. G., Danabasoglu, G., et al. ,2019: High climate sensitivity in the Community Earth System Model Version 2 (CESM2). *Geophysical Research Letters*, **46**, 8329– 8337. https://doi.org/10.1029/2019GL083978

- Guzman, R., and Coauthors, 2017: Direct atmosphere opacity observations from CALIPSO provide new constraints on cloud-radiation interactions: GOCCP v3.0 OPAQ Algorithm. *J. Geophys. Res. Atmos.*, **122**, 1066–1085, https://doi.org/10.1002/2016JD025946.

- Hansen, J., A. Lacis, D. Rind, G. Russell, P. Stone, I. Fung, R. Ruedy, and J. Lerner, 1984: Climate sensitivity: Analysis of feedback mechanisms. *Geophysical Monograph Series*, J.E. Hansen and T. Takahashi, Eds., Vol. 29 of, American Geophysical Union, 130–163. https://doi.org/10.1029/GM029p0130

- Hartmann, D. L., and K. Larson, 2002: An important constraint on tropical cloud - climate feedback: TROPICAL CLOUD-CLIMATE FEEDBACK. *Geophys. Res. Lett.*, **29**, 12-1-12–14, https://doi.org/10.1029/2002GL015835.

- Held, I. M., and B. J. Soden, 2006: Robust Responses of the Hydrological Cycle to Global Warming. *Journal of Climate*, **19**, 5686–5699, https://doi.org/10.1175/JCLI3990.1.Hersbach, H., Bell, B., Berrisford, P., Hirahara, S., Horányi, A., Muñoz-Sabater, J., et al. (2020). The ERA5 global reanalysis. *Quarterly Journal of the Royal Meteorological Society*, **146**(730), 1999–2049. https://doi.org/10.1002/qj.3803

- Höjgård-Olsen, E., H. Brogniez, and H. Chepfer, 2020: Observed Evolution of the Tropical Atmospheric Water Cycle with Sea Surface Temperature. *J. Climate*, **33**, 3449–3470, https://doi.org/10.1175/JCLI-D-19-0468.1.

- Hourdin, F., Rio, C., Grandpeix, J.-Y., Madeleine, J.-B., Cheruy, F., Rochetin, N., et al. (2020). LMDZ6A: The atmospheric component of the IPSL climate model with improved and better tuned physics. *Journal of Advances in Modeling Earth Systems*, **12**, e2019MS001892. https://doi.org/10.1029/2019MS001892.

- Hu, Y., Vaughan, M., Liu, Z., Lin, B., Yang, P., Flittner, D., et al. (2007). The depolarization attenuated backscatter relation: CALIPSO lidar measurements vs. theory. *Optics Express*, **15**(9), 5327. https://doi.org/10.1364/OE.15.005327

- Kato, S., and Coauthors, 2018: Surface Irradiances of Edition 4.0 Clouds and the Earth's Radiant Energy System (CERES) Energy Balanced and Filled (EBAF) Data Product. *J. Climate*, **31**, 4501–4527, https://doi.org/10.1175/JCLI-D-17-0523.1.
- Kjellsson, J., 2015: Weakening of the global atmospheric circulation with global warming. *Clim Dyn*, **45**, 975–988, https://doi.org/10.1007/s00382-014-2337-8.
- Klein, S. A., and C. Jakob, 1999: Validation and Sensitivities of Frontal Clouds Simulated by the ECMWF Model. *MONTHLY WEATHER REVIEW*, **127**, 18.
- Krinner, G., and Coauthors, 2005: A dynamic global vegetation model for studies of the coupled atmosphere-biosphere system: DVGM FOR COUPLED CLIMATE STUDIES. *Global Biogeochem. Cycles*, **19**, https://doi.org/10.1029/2003GB002199.
- Lacour, A., H. Chepfer, M. D. Shupe, N. B. Miller, V. Noel, J. Kay, D. D. Turner, and R. Guzman, 2017: Greenland Clouds Observed in *CALIPSO* -GOCCP: Comparison with Ground-Based Summit Observations. *J. Climate*, **30**, 6065–6083, https://doi.org/10.1175/JCLI-D-16-0552.1.
- Lacour, A., and Coauthors, 2018: How Well Are Clouds Simulated over Greenland in Climate Models? Consequences for the Surface Cloud Radiative Effect over the Ice Sheet. *J. Climate*, **31**, 9293–9312, https://doi.org/10.1175/JCLI-D-18-0023.1.
- Loeb, N. G., and Coauthors, 2018: Clouds and the Earth's Radiant Energy System (CERES) Energy Balanced and Filled (EBAF) Top-of-Atmosphere (TOA) Edition-4.0 Data Product. *J. Climate*, **31**, 895–918, https://doi.org/10.1175/JCLI-D-17-0208.1.
- Lu, J., G. A. Vecchi, and T. Reichler, 2007: Expansion of the Hadley cell under global warming. *Geophys. Res. Lett.*, **34**, L06805, https://doi.org/10.1029/2006GL028443.
- Ma, J., S.-P. Xie, and Y. Kosaka, 2012: Mechanisms for Tropical Tropospheric Circulation Change in Response to Global Warming. *J. Climate*, **25**, 2979–2994, https://doi.org/10.1175/JCLI-D-11-00048.1.
- Madec G., R. Bourdallé-Badie, P.-A. Bouttier, C. Bricaud, D. Bruciaferri, D. Calvert, … M. Vancoppenolle, 2017: NEMO ocean engine (Version v3.6-patch). Notes Du Pôle De Modélisation De L'institut Pierre-simon Laplace (IPSL). Zenodo. http://doi.org/10.5281/zenodo.3248739
- Meehl, G. A., Senior, C. A., Eyring, V., Flato, G., Lamarque, J. F., Stouffer, R. J., Taylor, K. E., & Schlund, M. ,2020: Context for interpreting equilibrium climate sensitivity and transient climate response from the CMIP6 Earth system models. *Science Advances*, **6**(26), eaba1981. https://doi.org/10.1126/sciadv.aba1981
- Mitchell, J. F. B., C. A. Senior, and W. J. Ingram, 1989: C02 and climate: a missing feedback? *Nature*, **341**, 132–134, https://doi.org/10.1038/341132a0.
- Morrison, A. L., J. E. Kay, H. Chepfer, R. Guzman, and V. Yettella, 2018: Isolating the Liquid Cloud Response to Recent Arctic Sea Ice Variability Using Spaceborne Lidar Observations. *J. Geophys. Res. Atmos.*, **123**, 473–490, https://doi.org/10.1002/2017JD027248.
- Morrison, A. L., J. E. Kay ,W. R. Frey, H. Chepfer, and R. Guzman, 2019: Cloud Response to Arctic Sea Ice Loss and Implications for Future Feedback in the CESM1 Climate Model. *J. Geophys. Res. Atmos.*, **124**, 1003–1020, https://doi.org/10.1029/2018JD029142.
- Nam, C., Bony, S., Dufresne, J.-L., and Chepfer, H., 2012: The 'too few, too bright' tropical low-cloud problem in CMIP5 models, *Geophys. Res. Lett.*, **39**, L21801, https://doi.org/10.1029/2012GL053421.

- O'Gorman, P. A., and M. S. Singh, 2013: Vertical structure of warming consistent with an upward shift in the middle and upper troposphere: VERTICAL STRUCTURE OF WARMING. *Geophys. Res. Lett.*, **40**, 1838–1842, https://doi.org/10.1002/grl.50328.
- Olauson, J., 2018: ERA5: The new champion of wind power modelling? *Renewable Energy*, **126**, 322–331, https://doi.org/10.1016/j.renene.2018.03.056.
- Ramanathan, V., R. D. Cess, E. F. Harrison, P. Minnis, B. R. Barkstrom, E. Ahmad, and D. Hartmann, 1989: Cloud-Radiative Forcing and Climate: Results from the Earth Radiation Budget Experiment. *Science*, **243**, 57–63, https://doi.org/10.1126/science.243.4887.57.
- Riahi, K., and Coauthors, 2011: RCP 8.5—A scenario of comparatively high greenhouse gas emissions. *Climatic Change*, **109**, 33–57, https://doi.org/10.1007/s10584-011-0149-y.
- Ringer, M. A., and Coauthors, 2006: Global mean cloud feedbacks in idealized climate change experiments. *Geophys. Res. Lett.*, **33**, L07718, https://doi.org/10.1029/2005GL025370.
- Rousset, C., and Coauthors, 2015: The Louvain-La-Neuve sea ice model LIM3.6: global and regional capabilities. *Geosci. Model Dev.*, **8**, 2991–3005, https://doi.org/10.5194/gmd-8-2991-2015.
- Schneider, S. H., 1972: Cloudiness as a Global Climatic Feedback Mechanism: The Effects on the Radiation Balance and Surface Temperature of Variations in Cloudiness. *J. Atmos. Sci.*, **29**, 1413–1422, https://doi.org/10.1175/1520-0469(1972)029<1413:CAAGCF>2.0.CO;2.
- Schwalm R., S. Glendon, P. B. Duffy, 2020: RCP8.5 tracks cumulative CO2 emissions. *Proceedings of the National Academy of Sciences*, **117** (33) 19656-19657. https://doi.org/10.1073/pnas.2007117117
- Soden, B. J., I. M. Held, R. Colman, K. M. Shell, J. T. Kiehl, and C. A. Shields, 2008: Quantifying Climate Feedbacks Using Radiative Kernels. *Journal of Climate*, **21**, 3504–3520, https://doi.org/10.1175/2007JCLI2110.1.
- Stephens, G. L., 2005: Cloud Feedbacks in the Climate System: A Critical Review. *Journal of Climate*, **18**, 237–273, https://doi.org/10.1175/JCLI-3243.1.
- Su, H., J. H. Jiang, C. Zhai, T. J. Shen, J. D. Neelin, G. L. Stephens, and Y. L. Yung, 2014: Weakening and strengthening structures in the Hadley Circulation change under global warming and implications for cloud response and climate sensitivity: Circulation, Clouds, Climate Sensitivity. *J. Geophys. Res. Atmos.*, **119**, 5787–5805, https://doi.org/10.1002/2014JD021642.
- Swales, D. J., R. Pincus, and A. Bodas-Salcedo, 2018: The Cloud Feedback Model Intercomparison Project Observational Simulator Package: Version 2. *Geosci. Model Dev.*, **11**, 77–81, https://doi.org/10.5194/gmd-11-77-2018.
- Taylor, K. E., M. Crucifix, P. Braconnot, C. D. Hewitt, C. Doutriaux, A. J. Broccoli, J. F. B. Mitchell, and M. J. Webb, 2007: Estimating Shortwave Radiative Forcing and Response in Climate Models. *Journal of Climate*, **20**, 2530–2543, https://doi.org/10.1175/JCLI4143.1.
- Taylor, K. E., R. J. Stouffer, and G. A. Meehl, 2012: An Overview of CMIP5 and the Experiment Design. *Bulletin of the American Meteorological Society*, **93**, 485–498, https://doi.org/10.1175/BAMS-D-11-00094.1.
- Vaillant de Guélis, T., H. Chepfer, V. Noel, R. Guzman, P. Dubuisson, D. M. Winker, and S. Kato, 2017a: The link between outgoing longwave radiation and the altitude at which a spaceborne lidar beam is fully attenuated. *Atmos. Meas. Tech.*, **10**, 4659–4685, https://doi.org/10.5194/amt-10-4659-2017.

- Vaillant de Guélis, T., H. Chepfer, V. Noel, R. Guzman, D. M. Winker, and R. Plougonven, 2017b: Using Space Lidar Observations to Decompose Longwave Cloud Radiative Effect Variations Over the Last Decade: Space lidar decomposes LWCRE variations. *Geophys. Res. Lett.*, **44**, 11,994-12,003, https://doi.org/10.1002/2017GL074628.
- Vaillant de Guélis, T., H. Chepfer , R. Guzman, M. Bonazzola, D. M. Winker, and V. Noel, 2018: Space lidar observations constrain longwave cloud feedback. *Sci Rep*, **8**, 16570, https://doi.org/10.1038/s41598-018-34943-1.
- Vancoppenolle, M., T. Fichefet, H. Goosse, S. Bouillon, G. Madec, and M. A. M. Maqueda, 2009: Simulating the mass balance and salinity of Arctic and Antarctic sea ice. 1. Model description and validation. *Ocean Modelling*, **27**, 33–53, https://doi.org/10.1016/j.ocemod.2008.10.005.
- Vecchi, G. A., and B. J. Soden, 2007: Global Warming and the Weakening of the Tropical Circulation. *Journal of Climate*, **20**, 4316–4340, https://doi.org/10.1175/JCLI4258.1.
- Vial, J., J.-L. Dufresne, and S. Bony, 2013: On the interpretation of inter-model spread in CMIP5 climate sensitivity estimates. *Clim Dyn*, **41**, 3339–3362, https://doi.org/10.1007/s00382-013-1725-9.
- Webb, M. J., and Coauthors, 2006: On the contribution of local feedback mechanisms to the range of climate sensitivity in two GCM ensembles. *Clim Dyn*, **27**, 17–38, https://doi.org/10.1007/s00382-006-0111-2.
- Webb, M. J., F. H. Lambert, and J. M. Gregory, 2013: Origins of differences in climate sensitivity, forcing and feedback in climate models. *Clim Dyn*, **40**, 677–707, https://doi.org/10.1007/s00382-012-1336-x.
- Wetherald, R. T., and S. Manabe, 1988: Cloud Feedback Processes in a General Circulation Model, *Journal of Atmospheric Sciences,* **45**, 8: 1397-1416, https://doi.org/10.1175/1520-0469(1988)045%3C1397:CFPIAG%3E2.0.CO;2
- Winker, D. M., M. A. Vaughan, A. Omar, Y. Hu, K. A. Powell, Z. Liu, W. H. Hunt, and S. A. Young, 2009: Overview of the CALIPSO Mission and CALIOP Data Processing Algorithms. *Journal of Atmospheric and Oceanic Technology*, **26**, 2310–2323, https://doi.org/10.1175/2009JTECHA1281.1.
- Winker, D., H. Chepfer, V. Noel, and X. Cai, 2017: Observational Constraints on Cloud Feedbacks: The Role of Active Satellite Sensors. *Surv Geophys*, **38**, 1483–1508, https://doi.org/10.1007/s10712-017-9452-0.
- Xu, K.-M., and Cheng, A., 2016: Understanding the tropical cloud feedback from an analysis of the circulation and stability regimes simulated from an upgraded multiscale modeling framework, J. Adv. Model. Earth Syst., 8, 1825-1846, https://doi.org/10.1002/2016MS000767.
- Yokohata, Tokuta & Emori, S. & Nozawa, Toru & Tsushima, Y. & Ogura, Tomoo & Kimoto, M., 2005. A simple scheme for climate feedback analysis. Geophysical Research Letters - GEOPHYS RES LETT. 32. 10.1029/2005GL023673.
- Zelinka, M. D., and D. L. Hartmann, 2011: The observed sensitivity of high clouds to mean surface temperature anomalies in the tropics: TEMPERATURE SENSITIVITY OF HIGH CLOUDS. *J. Geophys. Res.*, **116**, n/a-n/a, https://doi.org/10.1029/2011JD016459.
- Zelinka, M. D., S. A. Klein, and D. L. Hartmann, 2012a: Computing and Partitioning Cloud Feedbacks Using Cloud Property Histograms. Part I: Cloud Radiative Kernels. *J. Climate*, **25**, 3715–3735, https://doi.org/10.1175/JCLI-D-11-00248.1.

- Zelinka, M. D., S. A. Klein, and D. L. Hartmann, 2012b: Computing and Partitioning Cloud Feedbacks Using Cloud Property Histograms. Part II: Attribution to Changes in Cloud Amount, Altitude, and Optical Depth. *J. Climate*, **25**, 3736–3754, https://doi.org/10.1175/JCLI-D-11-00249.1.
- Zelinka, M. D., S. A. Klein, K. E. Taylor, T. Andrews, M. J. Webb, J. M. Gregory, and P. M. Forster, 2013: Contributions of Different Cloud Types to Feedbacks and Rapid Adjustments in CMIP5*. *Journal of Climate*, **26**, 5007–5027, https://doi.org/10.1175/JCLI-D-12-00555.1.
- Zelinka, M. D., C. Zhou, and S. A. Klein, 2016: Insights from a refined decomposition of cloud feedbacks: REFINED CLOUD FEEDBACK DECOMPOSITION. *Geophys. Res. Lett.*, **43**, 9259–9269, https://doi.org/10.1002/2016GL069917.
- Zelinka, M. D., T. A. Myers, D. T. McCoy, S. Po-Chedley, P. M. Caldwell, P. Ceppi, S. A. Klein, and K. E. Taylor, 2020: Causes of Higher Climate Sensitivity in CMIP6 Models. *Geophys. Res. Lett.*, **47**, https://doi.org/10.1029/2019GL085782.